https://doi.org/10.5194/wcd-2021-46
Preprint. Discussion started: 26 July 2021

Weather and Climate Dynamics Discussions
Open Access
EGU

Simulations of Bay of Bengal tropical cyclones in a regional convection-permitting atmosphere–ocean coupled model

Jennifer Saxby[1], Julia Crook[1], Simon Peatman[1], Cathryn Birch[1], Juliane Schwendike[1], Maria Valdivieso da Costa[2], Juan Manuel Castillo Sanchez[3], Chris Holloway[2], Nicholas P. Klingaman[2], Ashis Mitra[4], Huw Lewis[3]

[1]School of Earth and Environment, University of Leeds, UK
[2]National Centre for Atmospheric Science and Department of Meteorology, University of Reading, UK
[3]Met Office, UK
[4]National Centre for Medium Range Weather Forecasting, India

Correspondence to: Jennifer Saxby (jennifersaxby@outlook.com)

https://doi.org/10.5194/wcd-2021-46
Preprint. Discussion started: 26 July 2021

Abstract. Tropical cyclones (TCs) in the Bay of Bengal can be extremely destructive when they make landfall in India and Bangladesh. Accurate prediction of their track and intensity is essential for disaster management. This study evaluates simulations of Bay of Bengal TCs using a regional convection-permitting atmosphere-ocean coupled model. The Met Office Unified Model atmosphere-only configuration (4.4 km horizontal grid spacing) is compared with a configuration coupled to a three-dimensional dynamical ocean model (2.2 km horizontal grid spacing). Simulations of six TCs from 2016–2019 show that both configurations produce accurate TC tracks for lead times of up to 6 days before landfall. Both configurations underestimate high wind speeds and high rain rates, and overestimate low wind speeds and low rain rates. The ocean-coupled configuration improves landfall timing predictions and reduces wind speed biases relative to observations outside the eyewall but underestimates maximum wind speeds in the eyewall for the most intense TCs. The coupled configuration produces weaker TCs than the atmosphere-only configuration, consistent with lower sea surface temperatures in the coupled model and an overestimated cooling response in TC wakes. Both model configurations accurately predict rain rate asymmetry, suggesting a good representation of TC dynamics. Much of the rain rate asymmetry variation in the simulations is related to wind shear variations, with a preference for higher rain rates in the down-shear left quadrant.

https://doi.org/10.5194/wcd-2021-46
Preprint. Discussion started: 26 July 2021

Weather and Climate Dynamics Discussions
Open Access
EGU

1 Introduction

Tropical cyclones (TCs) are one of the most destructive weather phenomena. Accurate prediction of their track and intensity is essential for disaster management. The Bay of Bengal region of the northern Indian Ocean has a mean annual frequency of five TCs, in addition to less intense monsoon depressions (Rao et al., 2001). Their associated hazards, such as strong winds, heavy rainfall and storm surges, inflict substantial losses on India and Bangladesh's large coastal populations (Ali, 1999; Balaguru et al., 2014; Bandyopadhyay et al., 2018; Dasgupta et al., 2014; Mishra, 2014). During the past two centuries, 42% of global TC-related deaths were in Bangladesh and 27% in India. Cyclone Bhola in the Bay of Bengal in 1970 was the deadliest in history, with an estimated 300,000 deaths (Shultz et al., 2005). Reducing TC impacts requires accurate predictions of the storm track, intensity and size, several days before landfall.

Forecasts have improved at a rate of about one day per decade, such that modern 5-day TC track forecasts in global numerical weather prediction (NWP) models are as accurate as 1-day simulations were 40 years ago (Alley et al., 2019). Heming (2016) found that the global Met Office Unified Model (MetUM) had 3-day track errors comparable to 1-day errors in 1996. However, significant errors remain: TC position errors in the northern Indian Ocean are ~ 300 km at a lead time of 5 days in the global MetUM (Yamaguchi et al., 2017). Predictions of storm strength have improved much more slowly than track simulations (DeMaria et al., 2013). Efforts to increase TC prediction skill include improving observations to provide accurate initial and boundary conditions, resolving the complex physical processes driving TCs, ensemble forecasting (e.g. Titley et al., 2020), and increasing model resolution (e.g. Gentry and Lackmann, 2009). Most operational global NWP models have a horizontal grid length of about 10 km for the high-resolution deterministic runs and 15–25 km for ensemble systems, insufficient to resolve small scale processes influencing storm development (Hodges & Klingaman, 2019; Short & Petch, 2017). A more accurate representation of intense TCs would require horizontal resolution of a few km (Chen et al., 2007; Fierro et al., 2009; Gopalakrishnan et al., 2012), which allows explicitly represented, rather than parameterised, convection (Chan, 2005).

Air–sea interactions can influence cyclone tracks (Mandal et al., 2007) and moderate intensity (Emanuel, 1999). High TC surface wind stresses increase heat and moisture transfer to the atmosphere and cause vertical mixing of the upper ocean and upwelling by Ekman pumping (Mogensen et al., 2017; Shay et al., 2000). The ocean surface cools, reducing surface fluxes. Therefore, SST cooling in TC wakes reduces potential intensity, which is a theoretical limit on cyclone strength based on modelling the storm as a thermal heat engine (Bender et al., 1993; Bender & Ginis, 2000; Dutta et al., 2020; Schade & Emanuel, 1999). The impact of air–sea interactions is greater for high energy-transfer (i.e. intense or slow-moving) TCs, which cause more mixing-induced cooling (Neetu et al., 2019; Pothapakula et al., 2017; Vincent et al., 2012).

Air–sea coupled simulation is an established tool for modelling over longer timescales, such as seasonal forecasting and climate prediction, but it is also a rapidly developing tool for shorter timescales and more localised spatial scales (e.g. Lewis et al., 2019). Most previous studies show that air–sea coupling reduces TC intensity (Feng et al., 2019; Mogensen et al., 2017; Neetu et al., 2019; Takaya et al., 2010; Zarzycki, 2016;

https://doi.org/10.5194/wcd-2021-46
Preprint. Discussion started: 26 July 2021

Vellinga et al., 2020). Regional-scale coupled predictions are already operational for some TC cases in the Atlantic and North Pacific (Biswas et al., 2018; Jin et al., 2013; Saito et al., 2006), although the models used in these studies do not explicitly resolve convection. Fewer studies assess air–sea coupled models in the Bay of Bengal; the majority use mesoscale models with parameterised convection (Agrawal et al., 2020; Baisya et al., 2020; Greeshma et al., 2019; Yesubabu et al., 2020). They show a high sensitivity of TCs to air–sea interactions (Prakash & Pant, 2017), ocean mixed layer depth (Yesubabu et al., 2020) and ocean eddies (Anandh et al., 2020). Ocean coupling in mesoscale models generally improves TC track and intensity predictions (Greeshma et al., 2019; Srinivas et al., 2016; Yesubabu et al., 2020). Atmosphere-only (uncoupled) NWP models generally assume constant SST over the forecast, derived from ocean analysis systems, which has been the operational practice for TC prediction over the Bay of Bengal (Mohanty et al., 2015; Osuri et al., 2017; Routray et al., 2017; Srinivas et al., 2013; Nadimpalli et al., 2020). Updating SST during simulations with SST observations has been shown to improve track and intensity predictions (Mohanty et al., 2019; Rai et al., 2019). In an operational setting, it is possible to use the forecast SST from a regional ocean model as an updating lower boundary condition (Mahmood et al., 2021), but this is not common operational practice.

The present study investigates the representation of Bay of Bengal TCs using the recently developed IND1 regional coupled prediction system (Castillo et al., in prep.) with horizontal grid spacings of 4.4 km (atmosphere) and 2.2 km (ocean), allowing explicit representation of atmospheric convection and ocean eddies. We simulate six TCs using both an air–sea coupled configuration and an atmosphere-only configuration with a daily updating observation-based SST analysis as a surface boundary condition. Multiple initialisation times are used to create time-lagged ensembles. The oceanic response to TCs in the coupled model is assessed by comparing simulations with SST observations from fixed buoys and free-drifting floats. Evaluation of the simulations focuses on storm track and intensity, assessed using near-surface wind speeds and minimum mean sea level pressure (MSLP). The intensity and structure of near-surface winds and rainfall are used to evaluate atmospheric hazards. Ocean dynamics and oceanic hazards such as storm surges will be addressed in another study. Simulation diagnostics are compared to a range of observational and reanalysis datasets to evaluate model performance. Possible reasons for differences in TC predictions between the two model configurations, and relative to observations, are discussed.

2 Data and methodology

2.1 Model configurations

TC simulations were run using two research configurations of the IND1 regional scale modelling framework. The first configuration is uncoupled (atmosphere-only simulations, hereafter referred to as ATM), comprising a 4.4 km horizontal resolution implementation of the Met Office Unified Model (MetUM) atmosphere model, using the RAL1-T science configuration (Bush et al., 2020) with 80 vertical levels and a maximum altitude of 38.5 km (e.g. Brown et al., 2012). The land surface is represented by the Joint UK Land Environment Simulation (JULES) land surface model (Best et al., 2011; Clark et al., 2011). The MetUM atmosphere is forced with observed SST and sea ice analysis from the Operational Sea-surface Temperature and sea Ice Analysis

https://doi.org/10.5194/wcd-2021-46
Preprint. Discussion started: 26 July 2021

(OSTIA; Donlon et al., 2012). Most operational forecasts are run with fixed SST (e.g. Routray et al., 2017). However, the simulations in this study are significantly longer than would be run operationally, and so a fixed SST assumption is not valid. Therefore, SST is re-initialised each day in ATM. To provide a fair benchmark against which to compare coupled simulations, the SST is updated daily with the OSTIA product representative of the previous day's SST, as OSTIA data for each day is available for operational use the morning of the following day.

The second configuration (ocean coupled simulations, hereafter referred to as CPL) consists of an identical version of the MetUM and JULES components at 4.4 km resolution, coupled to the Nucleus for European Modelling of the Oceans (NEMO) dynamical ocean model (Madec Gurvan et al., 2019), through the OASIS3-MCT coupling libraries (Ocean Atmosphere Sea Ice Soil, version 2.0; Valcke et al., 2015). The NEMO model has a 2.2 km horizontal resolution and 75 vertical levels. Surface fluxes are exchanged as hourly mean values every hour throughout the forecast. The regional ocean component in CPL is free-running and is initialised from a free-running ocean-only spin up run; there is no local data assimilation within the model domain in either the forecast or the spin-up run.

In both configurations, atmospheric lateral boundary conditions are obtained from the global MetUM, which itself is re-initialised every day from the MetUM global analysis. Therefore, the simulations in this study are not forecasts, and this process could not be applied operationally. This setup is expected to result in lower TC track errors than if a free-running forecast was used to provide atmospheric lateral boundary conditions, as forecast motion errors are primarily driven by errors in the large-scale environmental wind field (Galarneau and Davis, 2012). The model runs are configured in this way to support the evaluation of model TC intensity and structure compared to observations, without the complication of track locations and timings that are far removed from reality. Details of the model components and boundary conditions are given in Table 1. For further information on the IND1 modelling framework, see Castillo et al. (in prep).

Table 1. Model configurations and components.

Configuration	**Atmosphere/land only (ATM)**	**Coupled (CPL)**
Description	Regional atmosphere/land configuration comprising MetUM atmosphere model (version 11.1) and JULES land surface model (version 5.2).	Atmosphere/land-ocean coupled configuration comprising MetUM atmosphere model (version 11.1) and JULES land surface model (version 5.2) coupled to NEMO ocean model (version 4.0.1) using OASIS3-MCT coupling library.
Resolution of model components	UM/JULES: 4.4 km horizontal resolution, 80 vertical levels	UM/JULES: 4.4 km horizontal resolution, 80 vertical levels NEMO: 2.2 km horizontal resolution, 75 vertical levels

https://doi.org/10.5194/wcd-2021-46
Preprint. Discussion started: 26 July 2021

Atmosphere/land initial analysis and boundary conditions	The global MetUM configuration (Walters et al., 2019) which is re-initialised daily from the MetUM global analysis.	The global MetUM configuration (Walters et al., 2019) which is re-initialised daily from the MetUM global analysis.
Ocean initial analysis and boundary conditions	Global OSTIA SST (Donlon et al., 2012). Updated daily at 00:00 during simulations.	Ocean initial state from free-running ocean-only IND1 configuration (named IND1o-e in Castillo et al., in prep); the free-running ocean run is initialised from rest conditions on 1st January 2016, with initial conditions and daily updated horizontal boundary conditions obtained from CMEMS global analysis.
Model time step	UM/JULES: 120 seconds	UM/JULES: 120 seconds NEMO: 90 seconds Coupling frequency: hourly
Diagnostic output times	Hourly (2D fields), 3-hourly (3D fields).	Hourly (2D fields), 3-hourly (3D fields).

2.2 TC case studies

Six TCs in the Bay of Bengal from 2016–2019, with various track and intensity characteristics (Figure 1), were selected for analysis. Four storms (Titli, Vardah, Gaja and Phethai) occurred in the post-monsoon TC season (late September to December), while two (Fani and Roanu) occurred during the pre-monsoon season (April–June). Maximum intensities range from a Category 5 TC (Fani) to less intense tropical storms (Roanu and Phethai); see Table 2 for details. Simulations were performed with ATM and CPL for simulation periods of between 4 and 13 days to cover the relevant period of TC evolution in each case. For each storm, deterministic simulations were initialised at 00:00 UTC on five consecutive days during storm evolution (four for TC Titli) to create time-lagged forecast ensembles, with each ensemble member having different initial conditions due to the initialisation time difference (Table 2). The end time is the same for all lagged ensemble members for each case study. TC track errors and errors in minimum MSLP and maximum wind speed were analysed for all simulations; a summary of errors for all simulations is given in Supplementary Table S1. However, most of the analysis in this study focuses on process evaluation. For this purpose, there is limited value in including data where simulated TC tracks are so far from observed tracks that comparison with observations is not relevant. Therefore, only results where tracks were within ~ 500 km of observed tracks throughout the simulation and made landfall within +/- 1 day of observed landfall were included when making quantitative comparisons to observations for the purpose of process evaluation. Simulations with large track errors or poor landfall timing, which are excluded from this process evaluation, are marked with an asterisk in Table 2. If a simulation from either ATM or CPL meets these exclusion criteria, the simulation initialised on the same date from the other configuration was also excluded. Inaccurate simulations are excluded from the analysis presented in Figures 6–11.

https://doi.org/10.5194/wcd-2021-46
Preprint. Discussion started: 26 July 2021

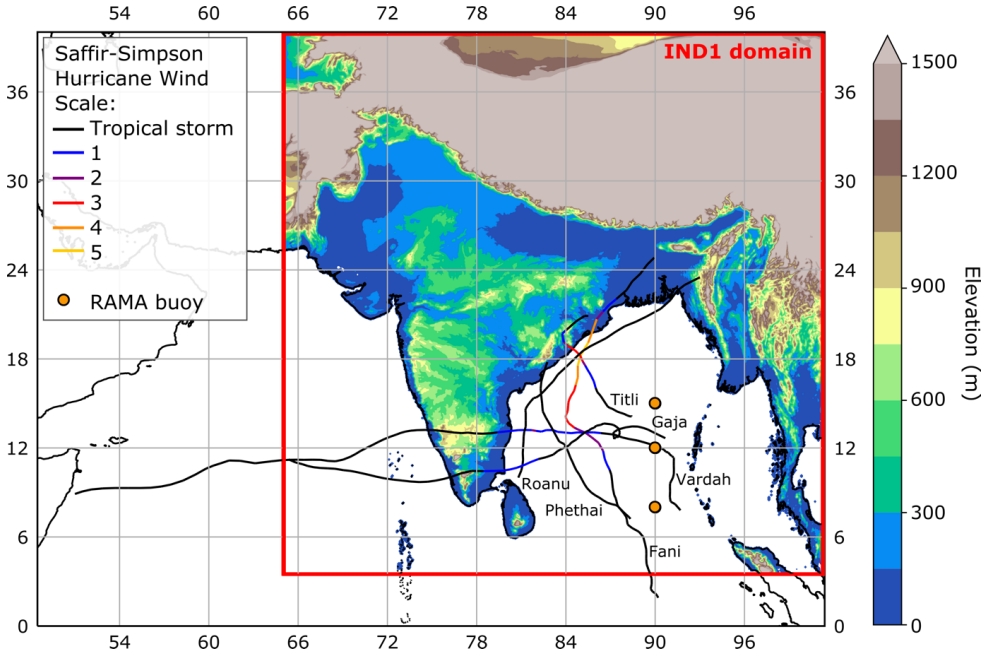

Figure 1. Map showing model domain (red box), model orography, and observed storm tracks and intensity from the IBTrACS archive. Saffir-Simpson Hurricane Wind Scale categories are based on USA IBTrACS data. Orange circles indicate RAMA buoys used for SST validation.

Table 2. Storm case study properties. * are simulations with poor landfall timing and/or large track errors, which are included in analysis of track and intensity errors but excluded from process evaluation (Figures 6-11). Saffir-Simpson Wind Scale categories are based on USA IBTrACS data.

Name	*Duration in IBTrACS*	*Simulations initialised (dd/mm/yyyy); all at 00:00.*	*Simulation end (dd/mm/yyyy); all at 00:00*	*Length of runs (days)*	*Landfall (state or district, country)*	*Origin in Bay of Bengal*	*Saffir-Simpson Category*
Fani	27th April – 3rd May 2019	26/04/2019 27/04/2019 28/04/2019 29/04/2019 30/04/2019	05/05/2019	5-9	Odisha, India	South	5
Titli	8th – 12th October 2018	06/10/2018 07/10/2018 08/10/2018 09/10/2018	16/10/2018	7-10	Andhra Pradesh, India	Central	3

https://doi.org/10.5194/wcd-2021-46
Preprint. Discussion started: 26 July 2021

Vardah	6th – 19th December 2016	05/12/2016* 06/12/2016* 07/12/2016 08/12/2016 09/12/2016	15/12/2016	6-10	Tamil Nadu, India	Southeast	2
Gaja	10th – 19th November 2018	10/11/2018* 11/11/2018 12/11/2018* 13/11/2018* 14/11/2018	23/11/2018	9-13	Tamil Nadu, India	East	1
Roanu	17th – 22nd May 2016	14/05/2016* 15/05/2016* 16/05/2016* 17/05/2016* 18/05/2016	24/05/2016	6-10	Chittagong, Bangladesh	West	Tropical storm
Phethai	13th – 18th December 2018	12/12/2018 13/12/2018 14/12/2018 15/12/2018 16/12/2018	20/12/2018	4-8	Andhra Pradesh, India	South	Tropical storm

2.3 Observations and reanalysis data

TC simulations were evaluated against a range of freely available observational and atmospheric reanalysis datasets (Table 3). TC track and intensity predictions were validated against the International Best Track Archive for Climate Stewardship (IBTrACS; Knapp et al., 2010), which is a merged archive of TC tracks and intensities as observed by the World Meteorological Organization (WMO) Regional Specialized Meteorological Centres (RSMCs) and other TC agencies. Agencies apply different observational algorithms, leading to discrepancies in track and intensity. For the TCs in this study, data from two agencies are available: RSMC New Delhi, part of the India Meteorological Department, and the USA's National Oceanic and Atmospheric Administration. Track positions from the two agencies generally agree well, so we compare the simulations to the average of the two. We compare forecast storm intensity to both available intensity estimates.

In addition to IBTrACS maximum wind speed, wind speed observations were obtained from the global SYNOP archive of surface synoptic land and ship-based observations. Precipitation analyses were taken from the multi-satellite GPM-IMERG gridded product (Huffman et al., 2020).

In-situ observed SSTs were obtained as time series from three RAMA (Research Moored Array for African-Asian-Australian Monsoon Analysis and Prediction; McPhaden et al., 2009) moored buoys in the Bay of Bengal. Buoy locations are shown in Figure 1. SST measurements were also obtained from Argo floats (Argo,

https://doi.org/10.5194/wcd-2021-46
Preprint. Discussion started: 26 July 2021

2020). Argo data consist of vertical profiles from free-drifting floats. Temperature is almost constant in the upper 10 m of each profile used here (not shown), and therefore we assumed that the uppermost measurement of each profile represented the foundation SST (Donlon et al., 2012) if it was within 10 m of the sea surface.

195 ERA5 reanalysis, the fifth generation of ECMWF atmospheric global climate reanalyses (Hersbach et al., 2020), was used in addition to in-situ observations. Since 2007, ERA5 SSTs are derived from OSTIA. ERA5 wind speeds on pressure levels were used to compute vertical wind shear along TC tracks.

Table 3. Summary of observational and reanalysis datasets used in this study, with a description of the variables
200 obtained.

Observational product	*Description*	*Variables*	*Resolution (temporal; spatial)*	*Source*
IBTrACS	NOAA's International Best Track Archive for Climate Stewardship	TC position, maximum sustained wind speed (10 min average at 10 m elevation), minimum sea level pressure	3-hourly; n/a	NOAA (Knapp et al., 2018)
ERA5	Atmospheric reanalysis	200 hPa and 850 hPa winds, sea surface temperature (foundation SST)	Hourly; 0.25° x 0.25°, 37 pressure levels	ECMWF; Copernicus Climate Data Store (Hersbach et al., 2018a, 2018b)
RAMA	Moored buoys (locations in Figure 1)	Sea surface temperature (at ~1 m depth)	10 minute or hourly (highest available resolution, varies by buoy and date); n/a	NOAA/PMEL (McPhaden et al., 2009).
Argo	Free-drifting profiling floats	Sea surface temperature (variable depth, within upper 10 m)	Floats surface every 10 days; n/a	Global Data Assembly Centre (Argo GDAC; Argo, 2020)
SYNOP	Sea based station reports (ships, rigs, platforms and moored buoys); land based station reports	Sustained wind speed (10 min average at 10 m elevation)	Hourly or 3-hourly; n/a	Met Office MetDB archive (Met Office, 2008a, 2008b)

https://doi.org/10.5194/wcd-2021-46
Preprint. Discussion started: 26 July 2021

IMERG	Multi-satellite precipitation product (microwave and IR) from GPM constellation; version V06B	Hourly-accumulated precipitation rate within a half-hour window (precipitationCal)	Half-hourly; 0.1° x 0.1°	NASA (Huffman et al., 2014)

2.4 TC tracking and analysis

TCs were identified and tracked hourly in the regional simulations using an objective feature-tracking methodology based on Nguyen et al. (2014). The method searches for minimum MSLP within 2.5° of the cyclone centre at the last output time and calculates the new TC centre based on a pressure centroid centred on this minimum and with a radius which is 80% of the radius of maximum winds at 10 m (J. Ashcroft, personal communication, 2020). If the newly calculated centre is more than 2.5° from the previous centre, the track stops, ensuring the storm is not tracked when the centre is unclear due to the storm breaking up. To verify this approach, TC Fani was also tracked using the objective tracking algorithm TRACK (Hodges, 1995), which tracks the maximum vertical average of vorticity between 850 and 600 hPa. The two methods produced similar results (not shown).

The majority of our analysis uses simulation data relative to the diagnosed cyclone track, where a track could be identified in model output. For simulations where the cyclone had formed at the start of the run, data prior to T+12 h was discarded to remove sensitivity to model spin-up.

To compare CPL and ATM track errors and perform statistical significance testing, matching times in IBTrACS and the simulations were found such that the number of data points and times used from each simulation ensemble member was the same in ATM and CPL. This allowed paired t-tests to be performed on the absolute errors and p-values obtained for the null hypothesis (no difference), the ATM less than hypothesis (significantly lower error in ATM than in CPL) and the CPL less than hypothesis (significantly lower error in CPL than in ATM). This analysis used as much of the tracks as possible. Mean absolute errors and RMSE over this time are quoted below and summarised in Supplementary Table S1, although Figures 2–4 in this manuscript show data for the whole track of each simulation.

TC intensity (maximum wind speed and minimum MSLP), at 3-hourly intervals, was verified against IBTrACS. Maximum wind speed in IBTrACS is a spatial maximum of the 10-minute sustained wind speed. The model 10 m wind field is not directly comparable to observed measurements of maximum sustained wind, but this is a standard comparison in model evaluation which, when applied consistently, indicates long-term trends in model accuracy (Heming, 2017). Model performance for simulating TC hazards was assessed by comparing simulated wind speed and rainfall to SYNOP and IMERG observations, respectively. Finally, the representation of TC dynamics was examined by comparing TC structure to ERA5/IMERG, using vertical wind shear (200–850 hPa), inner (< 250 km) and outer (250–500 km) rain rates and the asymmetry of inner rain rates as diagnostics.

https://doi.org/10.5194/wcd-2021-46
Preprint. Discussion started: 26 July 2021

235

3 Results

3.1 Tropical cyclone track errors

Track errors are low, even at long lead times, and are similar in the two model configurations (Figures 2 and 3), with larger track differences between different initialisation dates for a given storm than between model configurations. Track errors are higher for those storms moving east to west, although this is dominated by the large errors in the early initialisations of Vardah. Most simulations have track errors < 400 km, with a maximum of ~ 1100 km (calculated relative to IBTrACS storm location at the same validity time). Tracks in CPL generally fall to the left (west for northward-moving TCs; south for westward-moving TCs) of tracks in ATM. This relative shift is expected as CPL produces SST cold wakes, which tend to be more pronounced to the right of the TC track, as, in the Northern Hemisphere, this is often the location of maximum wind speeds, and hence wind-driven mixing, due to the alignment of TC translation and primary circulation. Cooler SSTs to the right of the TC track drive the TC towards the relatively warmer SSTs to its left. The leftward displacement of TC tracks in CPL agrees with other studies of coupled models (Khain & Ginis, 1991; Wu et al., 2005), although some authors have also found rightward displacement (Bender et al., 1993) or both leftward and rightward displacement (Feng et al., 2019).

For the intense TCs Fani and Titli, track prediction errors are independent of the initialisation date, such that later initialisations do not provide better simulations than earlier initialisations. For Vardah, errors reduce in each subsequent simulation. Simulations initialised on the earliest date of 05/12/2016 have maximum position errors of 1021 km (ATM) and 1097 km (CPL), while those initialised on the latest date of 09/12/2016 have significantly reduced maximum errors of 132 km (ATM) and 141 km (CPL). Although the cross-track position errors for the earlier Vardah runs are small (Figure 2e), the absolute vector track errors are significant (Figure 3e–f) due to large along-track errors in the simulations. Therefore, the simulated tracks follow the observed track well, but the timing is inaccurate. The TCs in the earlier Vardah simulations move faster and make landfall sooner than in the observations. For Gaja, Roanu and Phethai, there is less of a link between the start date and position errors, but in all three cases, the simulation with the latest start date in each ensemble gives the most accurate TC position while the storm is over the ocean (Figure 3g–l). Apart from Fani and Titli, track errors are significantly lower in ATM than CPL as indicated by a paired t-test. For Fani the track errors are significantly better in CPL.

Both ATM and CPL produce accurate landfall times for the most intense cyclones, Fani and Titli, as well as Phethai (Figure 3a–d, k, l), but landfall timings for Vardah, Gaja and Roanu are less accurate. Landfall timing errors for all simulations and initialisation times range from 0–138 hours (absolute values) with a mean and RMSE of 25 and 43 hours respectively (ATM) or 23 and 41 hours (CPL), with no significant difference between ATM and CPL based on paired t-tests. Errors in landfall timing for Roanu are large (Figure 3i–j); however, due to the storm track following the east coast of India closely (Figure 2d), this is often due to small errors in cross-track position rather than large errors in TC translation speed. If Roanu is excluded, the range of landfall timing errors is 0–63 hours with a mean and RMSE of 13 and 20 hours, respectively (ATM) or 12 and 19 hours (CPL).

https://doi.org/10.5194/wcd-2021-46
Preprint. Discussion started: 26 July 2021

Weather and Climate Dynamics Discussions
Open Access
EGU

Simulations initialised closer to the landfall time generally give more accurate landfall times; the mean and RMSE for simulations initialised within four days of landfall are 7.1 and 8.6 hours (ATM) or 5.7 and 8.1 hours (CPL). Landfall position errors range from 9 km to 2062 km, with a mean and RMSE of 362 and 700 km, respectively, and no statistically significant difference between ATM and CPL based on paired t-tests. Excluding cyclone Roanu, landfall position errors range from 15 to 409 km (mean and RMSE of 130 and 157 km). A summary of simulation error statistics for all simulations, with significance of differences between ATM and CPL determined using paired t-tests, is given in Supplementary Table S1.

https://doi.org/10.5194/wcd-2021-46
Preprint. Discussion started: 26 July 2021

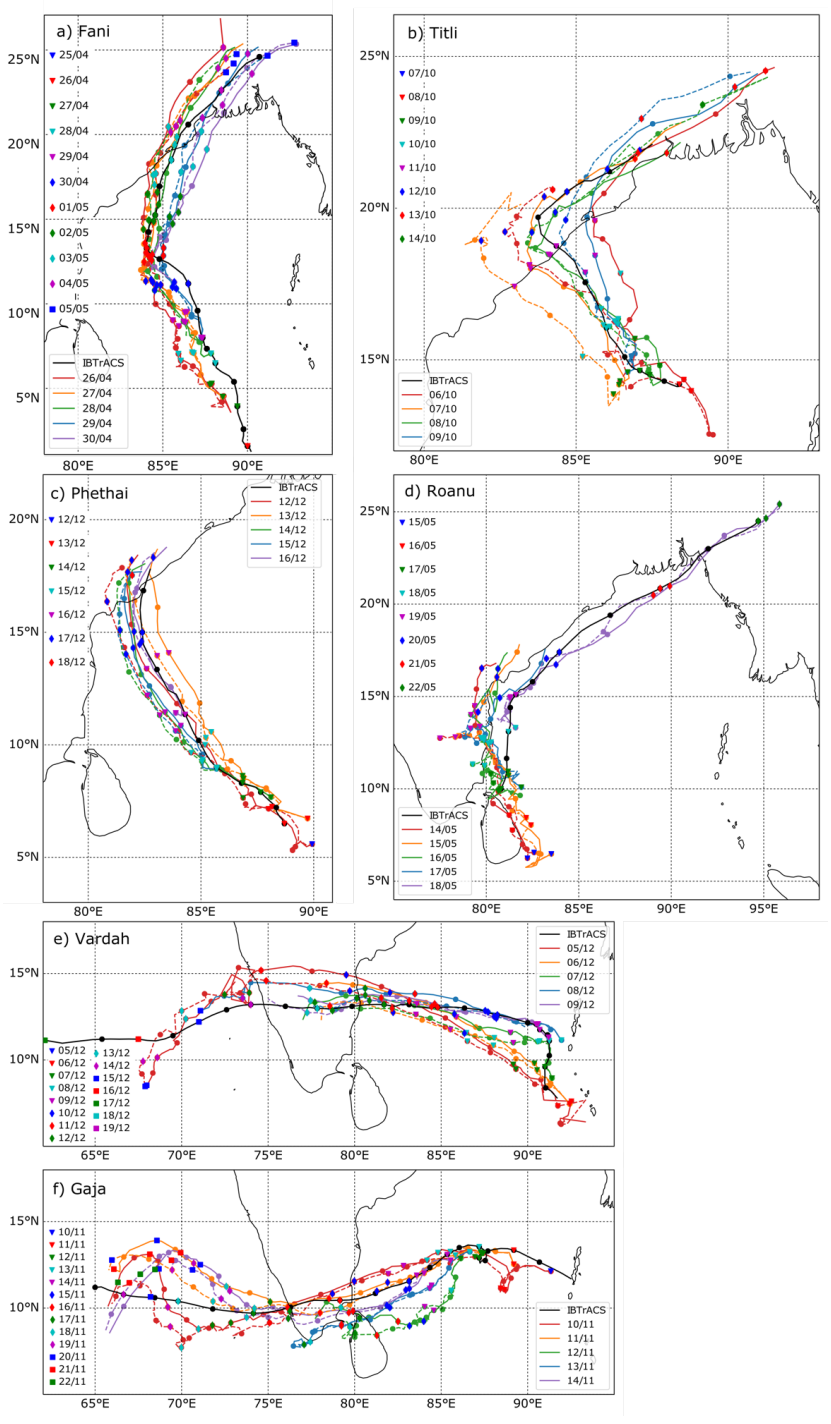

Figure 2. Simulated tracks for ATM (solid lines) and CPL (dashed lines), compared to IBTrACS (black line). Line colours indicate initialisation date (dd/mm).

https://doi.org/10.5194/wcd-2021-46
Preprint. Discussion started: 26 July 2021

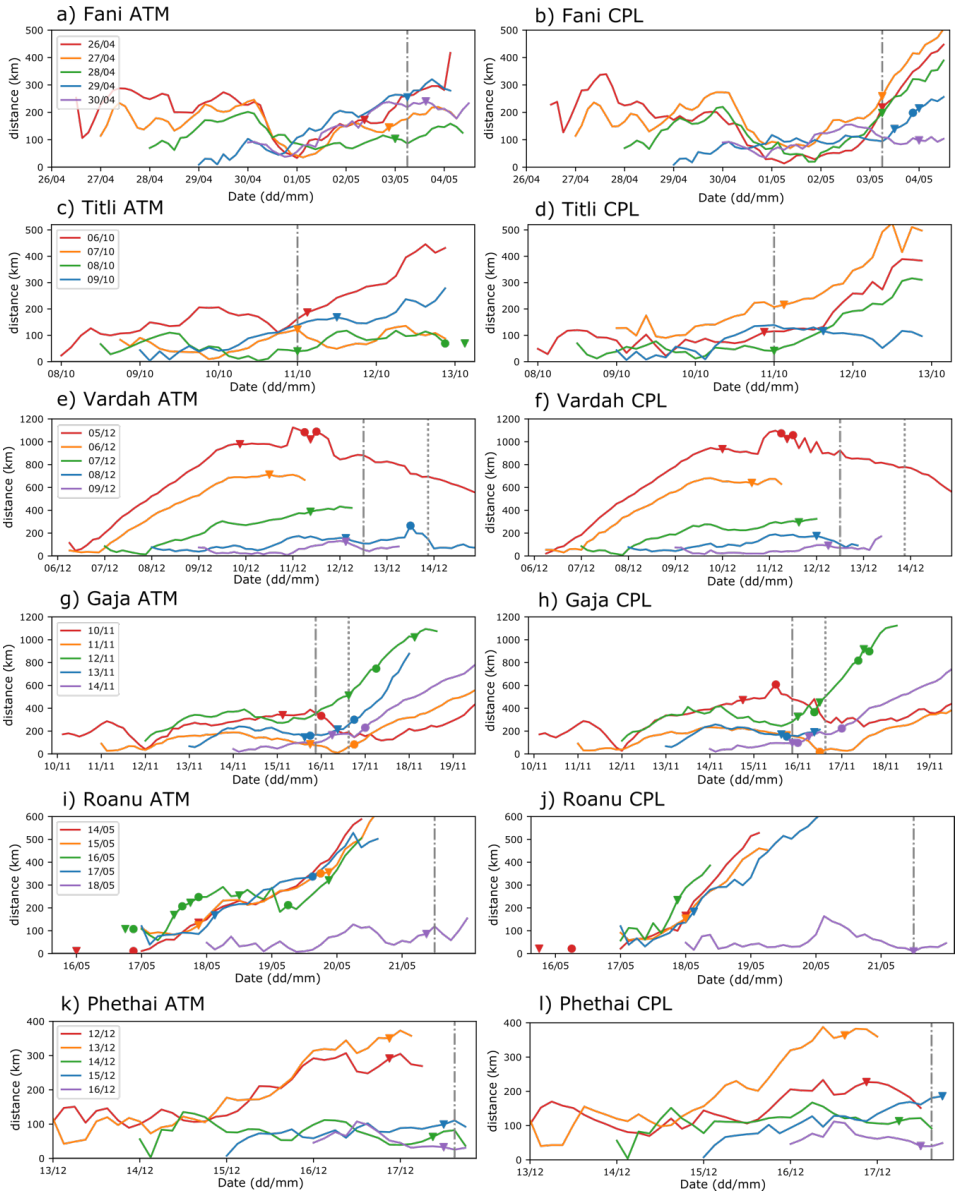

Figure 3. Simulation TC track error for ATM (left column) and CPL (right column) as distance relative to IBTrACS. Colours indicate initialisation date (dd/mm). Triangles indicate time of landfall; circles indicate re-emergence over the ocean. Dot-dash vertical line indicates time of landfall in IBTrACS; for Vardah and Gaja, the dotted line indicates time of re-emergence over the Arabian Sea in IBTrACS.

https://doi.org/10.5194/wcd-2021-46
Preprint. Discussion started: 26 July 2021

3.2 Tropical cyclone intensity

TC intensity was assessed using near-surface wind speeds, a critical hazard associated with landfalling TCs, and MSLP. In general, CPL predicts less intense storms (lower maximum wind speed and higher minimum MSLP) than ATM, which is expected as CPL simulates air–sea feedbacks which can lower SST and moderate intensity; the impact of coupling on SST is examined in Section 3.3.

Figure 4 shows the time series of maximum near-surface wind speeds in the eyewall from ATM, CPL and IBTrACS. For Fani, the most intense TC considered, both ATM and CPL underestimate peak maximum wind speed by up to ~ 35 m s^{-1} (Figure 4a–b) for the IBTrACS USA data and by up to ~15 m s^{-1} for IBTrACS New Delhi data. For cyclone Titli, peak wind speeds in ATM are lower than IBTrACS USA data but a good match to New Delhi data. Peak wind speeds in CPL are lower than those from either observing agency. The absolute wind errors over the whole Titli track compared to USA data are statistically significantly lower in ATM than CPL. For Vardah and Gaja, simulated and observed maximum winds agree well, but there are significant differences in the timing of peak intensities between the observations and simulations (Figure 4e–h). For these westward-moving storms the absolute error in maximum wind speeds over the whole track was statistically significantly lower in CPL than ATM for both agencies.

For Roanu, early initialisations make landfall too early to compare meaningfully with IBTrACS. For the last initialisation (18/05), both ATM and CPL accurately simulate maximum wind speed, with maximum wind speed error at the time of landfall < 10 m s^{-1} (Figure 4i–j). The intensity of Phethai is overestimated in both model configurations (Figure 4k–l) but is lower in CPL than ATM. However, absolute errors were not statistically significantly different between CPL and ATM (Supplementary Table S1).

Minimum MSLP time series are given in Supplementary Material (Figure S1). The errors in minimum MSLP biases are consistent with the errors in the maximum wind shown in Figure 4. CPL predicts lower intensity storms (higher minimum MSLP) than ATM. For the northward-moving storms, the absolute errors in minimum MSLP compared to USA data are significantly lower in ATM than CPL, but compared to New Delhi data are significantly lower in CPL than ATM. However, for the westward-moving storms the errors in minimum MSLP compared to both agencies are significantly lower in CPL than ATM.

https://doi.org/10.5194/wcd-2021-46
Preprint. Discussion started: 26 July 2021

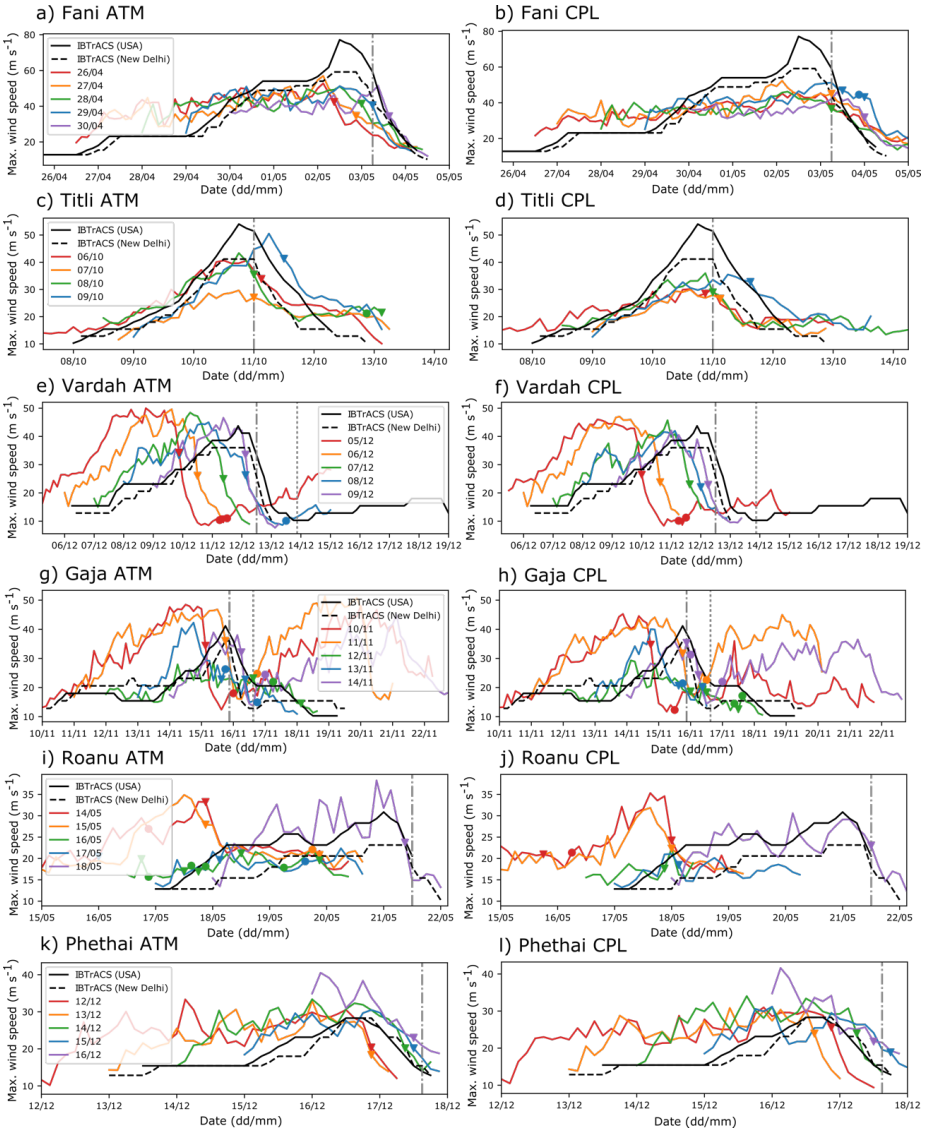

Figure 4. Maximum hourly instantaneous 10 m wind speed time series for ATM (left column) and CPL (right column), and maximum 10-minute sustained 10 m winds from IBTrACS. Colours indicate initialisation date (dd/mm). Triangles indicate time of landfall; circles indicate re-emergence over the ocean. Dash-dot vertical line indicates time of landfall in IBTrACS; for Vardah and Gaja, the dotted line indicates time of re-emergence over the Arabian Sea in IBTrACS.

Analysis of the wind-MSLP bias in ATM and CPL indicates that both models can accurately capture wind speed at higher MSLP but underestimate wind speed at lower MSLP (Figure 5). CPL storms do not reach the maximum intensity in IBTrACS (Figure 5) due to underestimating peak intensity for the strongest storms, as

https://doi.org/10.5194/wcd-2021-46
Preprint. Discussion started: 26 July 2021

Weather and Climate Dynamics Discussions
Open Access
EGU

shown in Figure 4 for wind speed. However, the wind-MSLP bias in CPL is overall lower than in ATM (Figure 5).

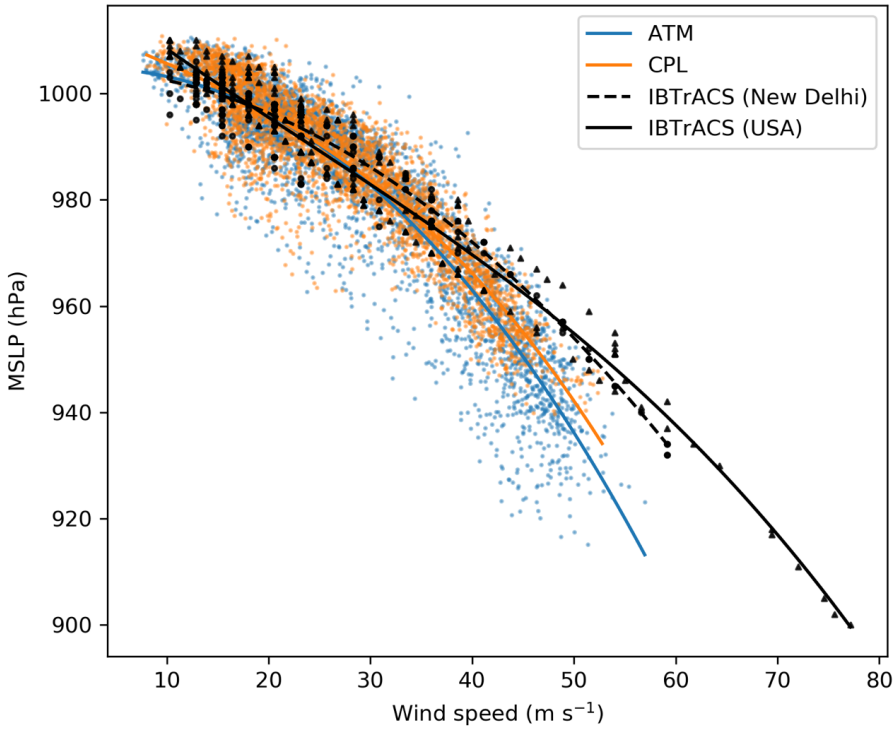

Figure 5. Minimum MSLP versus maximum 10 m wind speed at each diagnostic output time for ATM and CPL, compared to observations (IBTrACS; black dots indicate New Delhi data, triangles indicate USA data). All simulations are included.

Figure 4 shows lower peak intensity for intense cyclones and higher peak intensity for less intense cyclones in the simulations compared to IBTrACS. When the wind speed errors in the eyewall are binned by observed wind speed (Figure 6a-b), it is clear that this is symptomatic of a general tendency in the models to overestimate lower wind speeds and underestimate higher wind speeds. Both ATM and CPL underestimate the maximum wind speed for observations > ~ 35 m s^{-1}. As maximum wind speeds from IBTrACS are uncertain, indicated by the variation between USA and New Delhi measurements (Figure 4), wind speeds away from the TC centre were also compared to land- and ship-based SYNOP wind speed records, where observations within 500 km of the observed TC centre and within 30 minutes of the model output time were included in the comparison. The locations of the SYNOP observations used for each storm and time series from selected individual stations are shown in Supplementary Figures S2–S7. Figure 6c–d show similar errors to those seen in the eyewall when comparing the model to IBTrACS (Figure 6a–b). Both models overestimate lower wind speeds relative to SYNOP and underestimate wind speeds for observations > ~ 10 m s^{-1}. Consistent with the wind errors, the simulations have higher minimum MSLP than IBTrACS for observations < ~ 970 hPa and lower MSLP at

https://doi.org/10.5194/wcd-2021-46
Preprint. Discussion started: 26 July 2021

Weather and Climate Dynamics Discussions
Open Access
EGU

greater MSLP values (Figure 6e–f). Overall, the errors are similar in ATM and CPL, except for a slightly larger spread in error for ATM.

To assess the relationship between wind speed errors, forecast lead time and landfall, errors in simulated wind speed relative to SYNOP were averaged in 2D bins with dimensions of 24 h (forecast lead time) by 24 h (time relative to storm landfall). Errors generally increase with both forecast lead time and temporal proximity to landfall (Figure 7). Note that all bins have a positive mean error due to numerous SYNOP observations at low wind speeds (< 10 m s^{-1}), which the models tend to overestimate. Wind speed biases relative to SYNOP are generally lower in CPL than ATM.

https://doi.org/10.5194/wcd-2021-46
Preprint. Discussion started: 26 July 2021

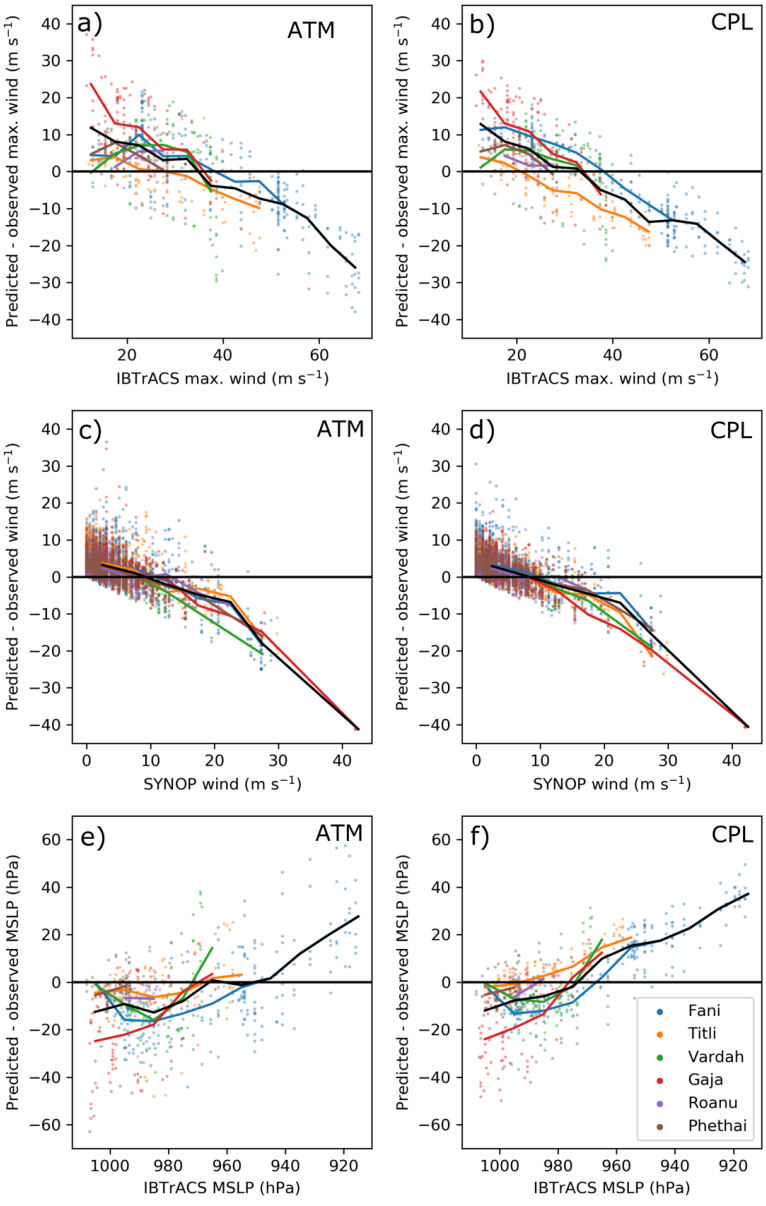

360

Figure 6. Wind speed and minimum MSLP error for ATM and CPL, relative to IBTrACS and SYNOP measurements. Lines are mean bias values for bins of 5 m s^{-1} (wind speed) or 10 hPa (MSLP). The black line shows the mean error for all case studies. Simulations with inaccurate tracks (marked with an asterisk in Table 2) are excluded.

https://doi.org/10.5194/wcd-2021-46
Preprint. Discussion started: 26 July 2021

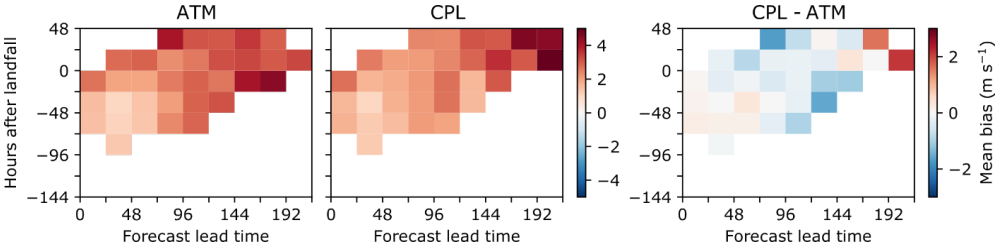

Figure 7. Mean bias of simulated wind speed compared to available land and ship SYNOP data for all lagged ensemble members and all storm case studies. Data are binned by forecast lead time, and time relative to landfall (24 hr x 24 hr bins). We use SYNOP observations within 500 km of the TC centre at each timestep. Observations are compared to wind speed at the same location (a single model grid cell) at the closest forecast time; all observations are within 30 minutes of the forecast output time. Bins containing < 50 measurements have been removed. Simulations with inaccurate tracks (marked with an asterisk in Table 2) are excluded.

3.3 Simulated SSTs and association with intensity biases

The passage of TCs across the Bay of Bengal leads to ocean cooling (Figure 8). Compared to observations from three fixed RAMA buoys (see Figure 1 for locations), CPL predicts the timing of SST minima well but typically produces a cold bias (Figure 8), with minimum SSTs too cold by up to ~ 1°C. TC Fani is an exception, with SST cooling underestimated at the 8°N buoy and overestimated at the 15°N buoy. The SST discrepancies are partly due to storm position errors, as the simulated cold wake is centred along the simulated track, and there is a sharp gradient in SST moving away from the track. Tracks for Fani in simulations are further from the 8°N RAMA buoy, compared to observed tracks, when the storm is at 8°N but closer to the 15°N buoy when the storm is at 15°N. The SST diurnal cycle phase and amplitude are reasonably well represented in CPL for most storms, but for Vardah and Gaja the amplitude is overestimated.

In comparison, ATM has a lag in the timing of SST cooling, which is associated with the use of the OSTIA product that would have been available for initialisation on a given day had these simulations been run in near real-time, which is the OSTIA product that represents the previous day's SST (see Section 2.1). ERA5, however, uses OSTIA SST applied to the relevant day (Hirahara et al., 2016). Therefore, the differences between ERA5 SST and ATM SST are due to the time difference in the OSTIA data used and the coarser resolution of ERA5. The magnitude of the SST cooling is generally underestimated in the ATM simulations relative to RAMA observations. Therefore, SST in ATM is generally too high. Using a daily analysis product as a surface boundary condition for fast-moving phenomena such as TCs will always induce a mismatch between observed and forcing SSTs. As TC-induced cooling can be ~ 2°C, ATM SST errors can also be as high as 2°C (Figure 8).

ATM and CPL use different ocean initial analysis and boundary conditions (OSTIA SST in ATM and a free-running ocean-only IND1 configuration in CPL; see Table 1), and ATM uses daily-updated SST observations. Therefore, we cannot determine whether SSTs in CPL are cooler than in ATM due to air-sea coupling or

https://doi.org/10.5194/wcd-2021-46
Preprint. Discussion started: 26 July 2021

experiment design. However, by analysing data from free-drifting Argo floats, which give good spatial coverage of the model domain, we can investigate TC-induced cooling by examining SST biases in the TC wakes. Figure 9 shows SST in ATM and CPL relative to the Argo float observations, with floats in the wake of a cyclone (defined as < 250 km from the observed storm track after the storm has passed) plotted using filled symbols. For locations of Argo floats, see Supplementary Figures S8-S9. ATM SSTs show a warm bias in the wake (for all storms except Gaja), which is expected because the daily updated SSTs from OSTIA are time-lagged, and in general, satellite SST products such as OSTIA are unable to represent TC cold wakes on the time scale required due to a lack of observations in the vicinity of TCs or insufficient inclusion of real-time observations (e.g. Liu et al., 2018). In the rest of the domain, away from wake regions, despite the lag between the validity of the OSTIA observations and the forecast time, ATM SSTs are generally accurate (mean biases range from -0.25°C to 0.02°C). CPL SSTs are too low throughout the domain and in the wake of the storm after its passage. For Titli, Vardah, Gaja and Phethai, the mean bias in the wake is greater than the mean bias outside the wake. For Fani, the mean SST bias in the wake is equal to that in the wider model domain, although the maximum SST biases occur in the TC wake. For Roanu, the mean SST bias in the wake is less than in the wider domain. SST bias is insensitive to forecast lead time (not shown) which is expected as the regional ocean initial condition in CPL is taken from subsequent days of the same long run. Compared to the wider model domain, the larger SST biases in TC wakes in CPL suggest an overestimation of TC-induced SST cooling in addition to cold SST biases throughout the domain. This bias is consistent with errors in ocean initialisation (too-cold upper-ocean temperatures) and a negative bias in net surface heat input into the ocean (Valdivieso et al., 2021). For most cyclones in this study, CPL underestimates peak intensity; it is expected that if the cold bias in SST were reduced, wind and MSLP could be better reproduced.

https://doi.org/10.5194/wcd-2021-46
Preprint. Discussion started: 26 July 2021

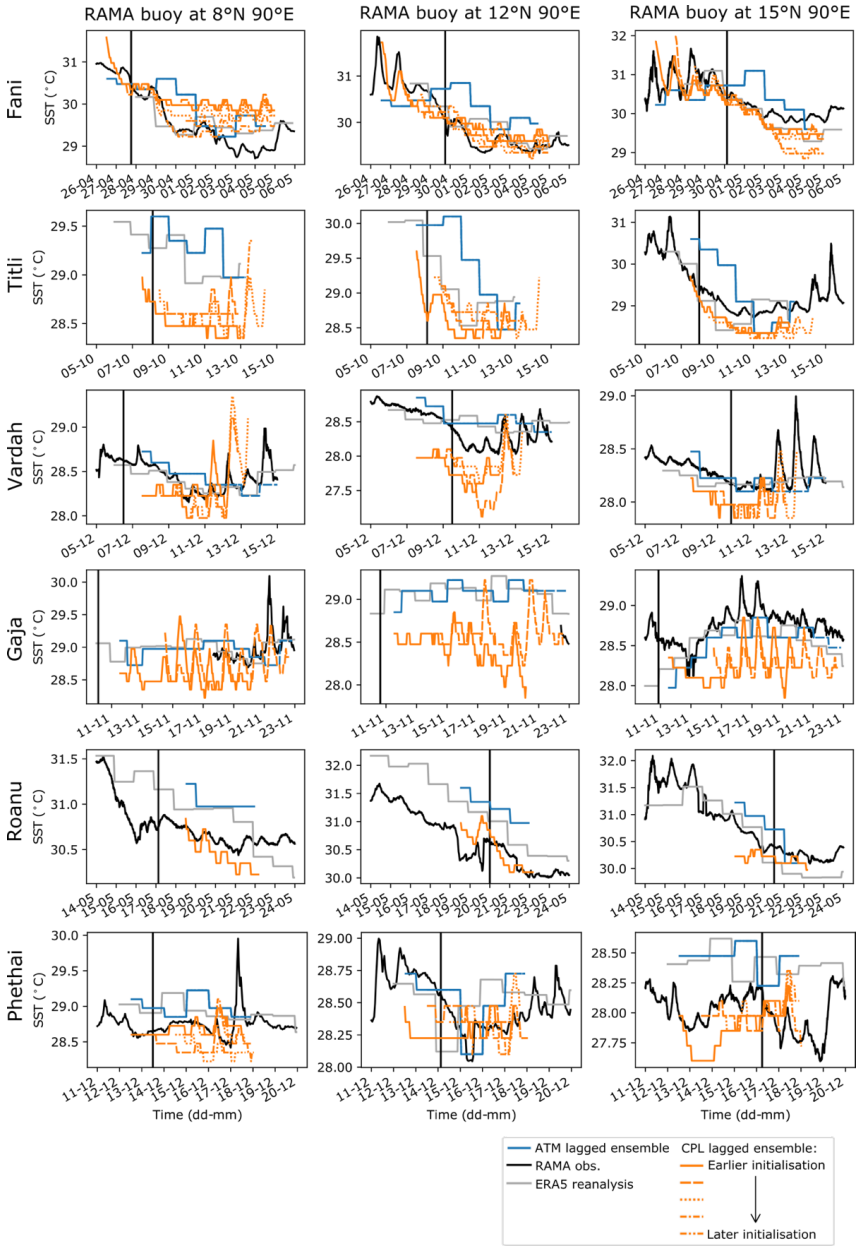

Figure 8. Hourly SST timeseries from three RAMA buoys in the Bay of Bengal (data from only one buoy available for TC Titli), compared to SST time series at the same location (nearest grid point of the models) for ATM, CPL and ERA5. The vertical line indicates the time at which the storm is nearest to the buoy in the observed track (IBTrACS). Time series are given for the duration of each time-lagged ensemble member, excluding the first 12 hours; simulations with different initialisation times are plotted with different line styles. For exact simulation initialisation dates, see Table 2. Simulations with inaccurate tracks (marked with an asterisk in Table 2) are excluded. Buoy locations are shown in Figure 1 and stated at the top of this figure.

https://doi.org/10.5194/wcd-2021-46
Preprint. Discussion started: 26 July 2021

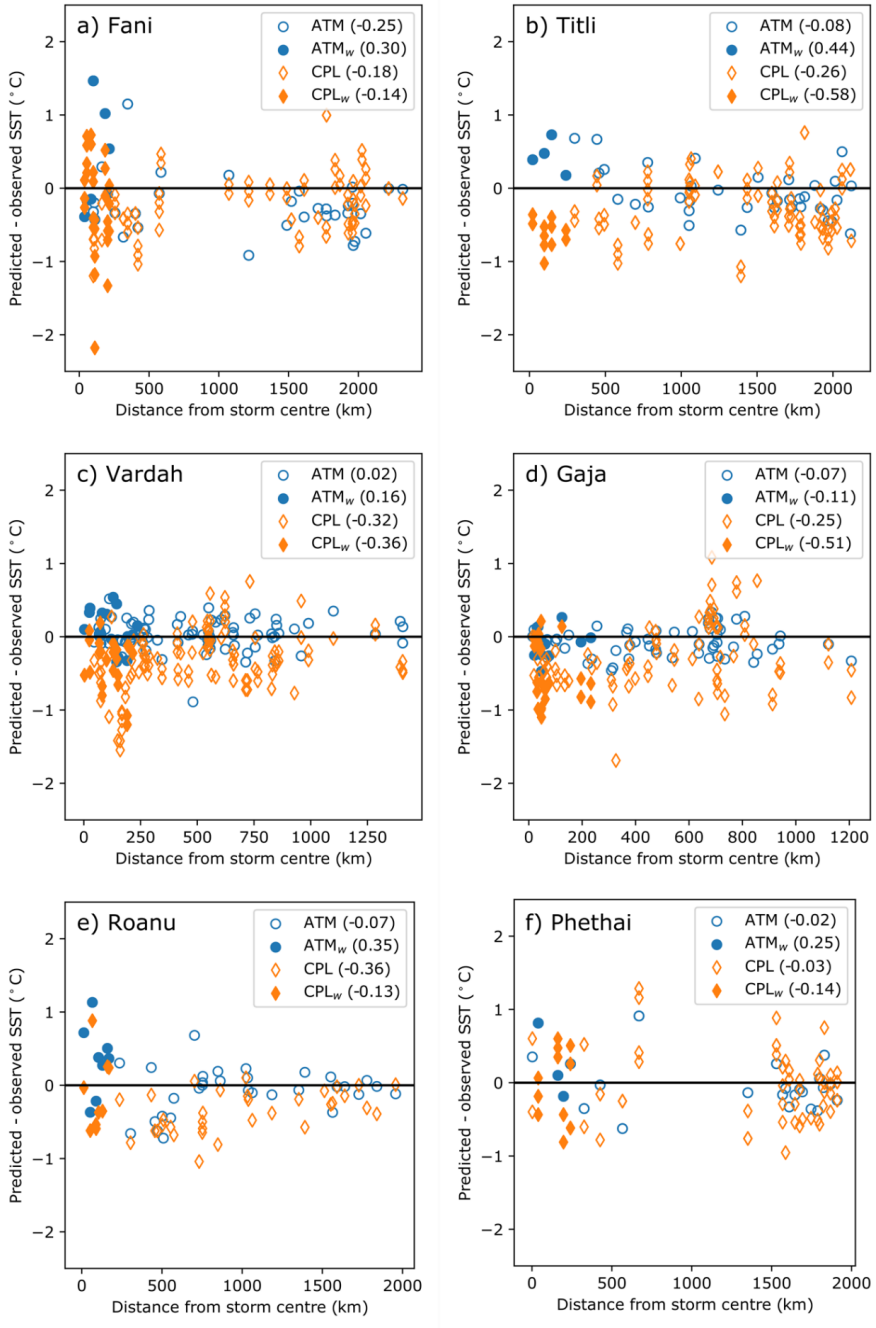

Figure 9. SST relative to Argo floats for the ATM and CPL simulations. Filled symbols indicate points within 250 km of the observed storm track after storm passage (the cyclone wake; subscript $_w$ in legend). Mean bias is summarised in parentheses. Simulations with inaccurate tracks (marked with an asterisk in Table 2) are excluded.

https://doi.org/10.5194/wcd-2021-46
Preprint. Discussion started: 26 July 2021

Weather and Climate Dynamics Discussions
Open Access
EGU

4 Cyclone structure

TC inner and outer rainfall, and inner rainfall asymmetry, are evaluated against satellite-derived rainfall retrievals (Figures 10–11). The radii for inner rainfall (250 km) and outer rainfall (250–500 km) are based on the radii used in Hence & Houze (2012), who found a distinction in the convective nature of rainfall inside and outside a radius of ~ 200 km. They found inner rainfall to be convective and stratiform, but outer rainfall was much more sparse and largely convective. The inner radius used here is larger than that used in many inner rainfall asymmetry studies (more typically ≤ 100 km) because this study looks at both pre- and post-landfall, and after landfall, the maximum rain rate radius is often > 100 km. Rainfall is averaged over the two hours centred on each 3-hourly tracking output time.

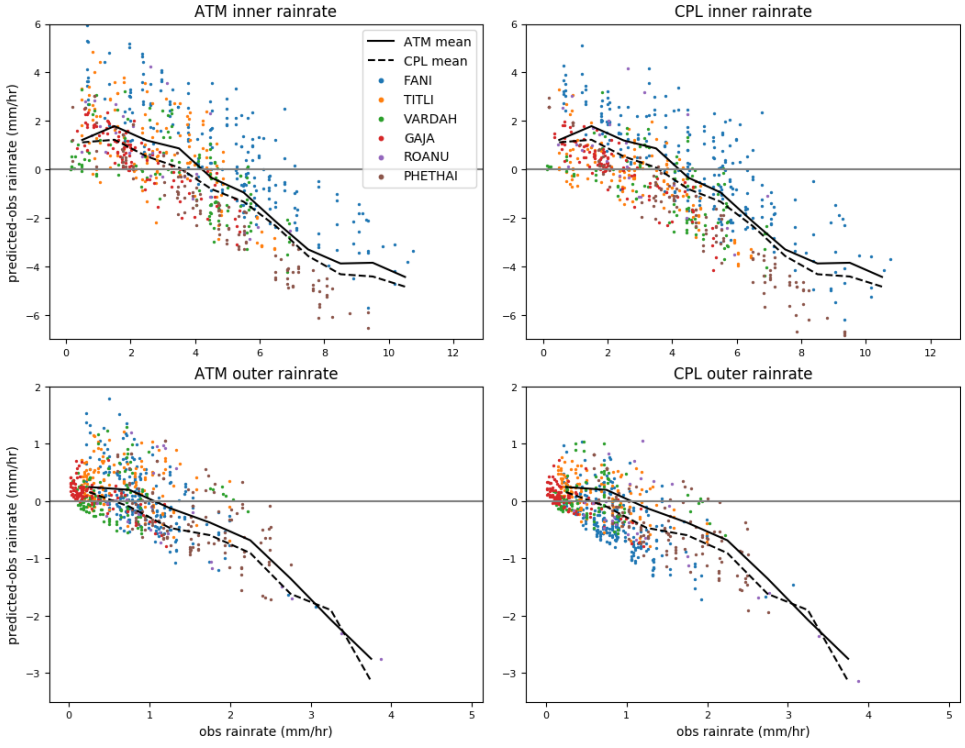

Figure 10. 2-hourly inner (within 250 km of the TC centre, top) and outer (250–500 km from the TC centre, bottom) rain rate bias in simulations against IMERG rain rate. Black lines show the mean of all simulations for ATM (solid) and CPL (dashed). Simulations with inaccurate tracks (marked with an asterisk in Table 2) are excluded.

Inner rain rates are much higher than outer rain rates in both simulations and observations (Figure 10, note different axis scales). Lower rain rates tend to be overestimated, and higher rain rates underestimated, in both CPL and ATM. The more intense storms in terms of maximum wind speeds tend to have higher simulated inner rain rates (up to ~ 9 mm/hr for Fani) than the least intense storms (up to ~ 4 mm/hr for Phethai), but this is not

https://doi.org/10.5194/wcd-2021-46
Preprint. Discussion started: 26 July 2021

the case in observations (up to ~ 10 mm/hr for Fani and ~ 9 mm/hr for Phethai). On average, rain rates are slightly lower in CPL than ATM (black dashed lines compared to black solid lines), possibly also due to the lower storm intensity (maximum wind speeds) in CPL. It was found that inner rain rates in IMERG tend to drop off once landfall has been made, so simulated inner rain rates are often lower than IMERG over the ocean but higher than IMERG over land. Rainfall biases over land may be related to high orography (near the Himalaya for Fani, Titli and Roanu and smaller areas of high orography in Tamil Nadu for Vardah and Gaja). The absolute error in inner rain rate over the whole time of the tracks (excluding simulations with inaccurate tracks, marked with an asterisk in Table 2) is significantly lower in CPL (1.6 mm/hr) than ATM (1.8 mm/hr) and this is largely due to the lower errors over land when rain rates are lower (see Supplementary Table S2).

TCs may display non-axisymmetric behaviour due to storm motion, environmental vertical wind shear, dry-air intrusions, interaction with mid-level and upper-level synoptic systems, and non-uniform surface characteristics resulting in asymmetric heating (Alvey III et al., 2015; Chan & Liang, 2003; Chen et al., 2006; Corbosiero & Molinari, 2003; DeHart et al., 2014; Frank & Ritchie, 1999; Shu et al., 2018; Thakur et al., 2018; Wang & Wu, 2004; Xu et al., 2014). These processes cause asymmetric distributions of rainfall and near-surface winds, both critical hazards to forecast. Asymmetric structures also impact TC intensity, with more symmetric structures tending to maintain intensity and asymmetric structures weakening (Wang & Wu, 2004). Our study concentrates on the asymmetry of rainfall due to the hazards associated with heavy rainfall. In this study, normalised north minus south and east minus west rain rate asymmetry were calculated for the inner rain rate (within 250 km of centre) for all TC cases.

Although high-frequency variability in rain rate asymmetry is not well captured, the simulations accurately predict daily changes over TC lifetimes (not shown). Inner rain rate asymmetry in the simulations generally matches that in observations, with Pearson correlation coefficients between 0.62 and 0.72 (see Supplementary Figure S10). The mean absolute errors for the N-S asymmetry are significantly lower in ATM (0.58) than CPL (0.60) due to differences over land. The E-W asymmetry has similar mean absolute errors but they are not significantly different in ATM and CPL. Errors can be due to timing errors in the simulations, such that one would not expect the environmental conditions to be the same. Studies show that vertical wind shear is a dominant control on rainfall asymmetry when shear is > 5 ms^{-1} and that rainfall tends to occur in the down-shear left quadrant (e.g. Alvey III et al., 2015; Chen et al., 2006; DeHart et al., 2014; Xu et al., 2014). Figure 11 shows the inner rain rate asymmetry vs the (200 hPa – 850 hPa) vertical wind shear calculated as a mean over the annulus 500–750 km from the storm centre. There is more rain north of the TC centre with larger northward wind shear in observations and simulations, and likewise more rain east of the TC centre with larger eastward shear, suggesting a preference for rain down-shear.

In the cases of TCs Fani and Roanu (spring, pre-monsoon), the vertical wind shear over the ocean is westwards to south-westwards (rear-left of storm motion) but becomes roughly north-eastwards (aligned with storm motion) where the storm makes landfall. In the other TC cases (winter, post-monsoon), the vertical wind shear is northwards to north-westwards (quite well aligned with storm motion) and rarely goes southwards. Therefore, the spring TCs (Fani and Roanu) occupy a different plot region than winter cyclones, and correlation

https://doi.org/10.5194/wcd-2021-46
Preprint. Discussion started: 26 July 2021

coefficients have been calculated separately. The high positive Pearson correlation coefficients show that inner rain rate asymmetry is primarily controlled by vertical wind shear in simulations and observations, with spring having a higher N-S correlation than winter because of the greater spread of meridional shear values. When simulated rain rate asymmetry did not match observed asymmetry well, this was often due to the different vertical wind shear at that time.

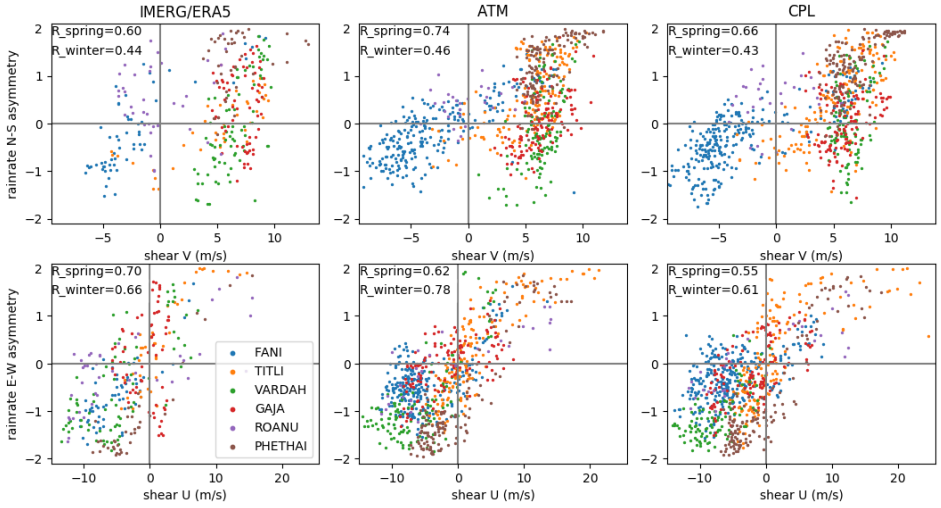

Figure 11. Inner rain rate asymmetry vs vertical wind shear for north minus south (top) and east minus west (bottom) and for observations (left), ATM (middle) and CPL (right). The Pearson correlation coefficients are given at the top of each panel for the storms in spring (Fani and Roanu) and in winter (all others). Simulations with inaccurate tracks (marked with an asterisk in Table 2) are excluded.

For pre-monsoon cyclones (Fani and Roanu), the shear over the ocean shifts from south-westwards (rear-left of the track) to north-eastwards (more aligned with the track) in observations and simulations around landfall. The shift occurs at landfall for Fani (still left of the track) and a day before landfall for Roanu (slightly right of the track). Both simulations and IMERG show a preference for rain to the rear-left of the centre before the shift and front-left afterwards (Figure 12a-c and 12m-o). The cross-track asymmetry after the shift in shear is more variable for Roanu. In CPL simulations of TC Fani, the rain shifts to the east (up-shear) immediately before landfall, although the shear in CPL is more to the south, suggesting shear is not the primary control on rainfall at this time. Fani is the only TC case where ATM and CPL show distinct differences in all initialisations.

For the post-monsoon cyclones during the day before landfall, shear is generally well aligned with or slightly to the right of the track, resulting in more rainfall to the front and often to the left in both simulations and observations. After landfall, the shear shifts more to the right. For the north-eastward moving storms (Titli and Phethai), the shear becomes stronger, resulting in more rain to the front and right in observations and simulations, although cross-track rain asymmetry is more variable in simulations than in observations (Figure 12d–f and 12p–r). For the westward-moving cyclones (Vardah and Gaja), the shear remains to the right of the

https://doi.org/10.5194/wcd-2021-46
Preprint. Discussion started: 26 July 2021

track but weakens in observations and simulations, resulting in variable rainfall asymmetry (Figure 12g–i and 12j–l).

When the shear is well aligned with the storm motion, the rain preference is clearly to the front, but slight differences in the shear direction, in the cyclonic wind speeds and the storm's life stage, can determine whether rain preference is to the right or left. When shear is not well aligned with the storm motion, the simulations more accurately match the observed cross-track asymmetry. In conclusion, ATM and CPL represent cyclone structure reasonably well, and there is little difference between model configurations.

https://doi.org/10.5194/wcd-2021-46
Preprint. Discussion started: 26 July 2021

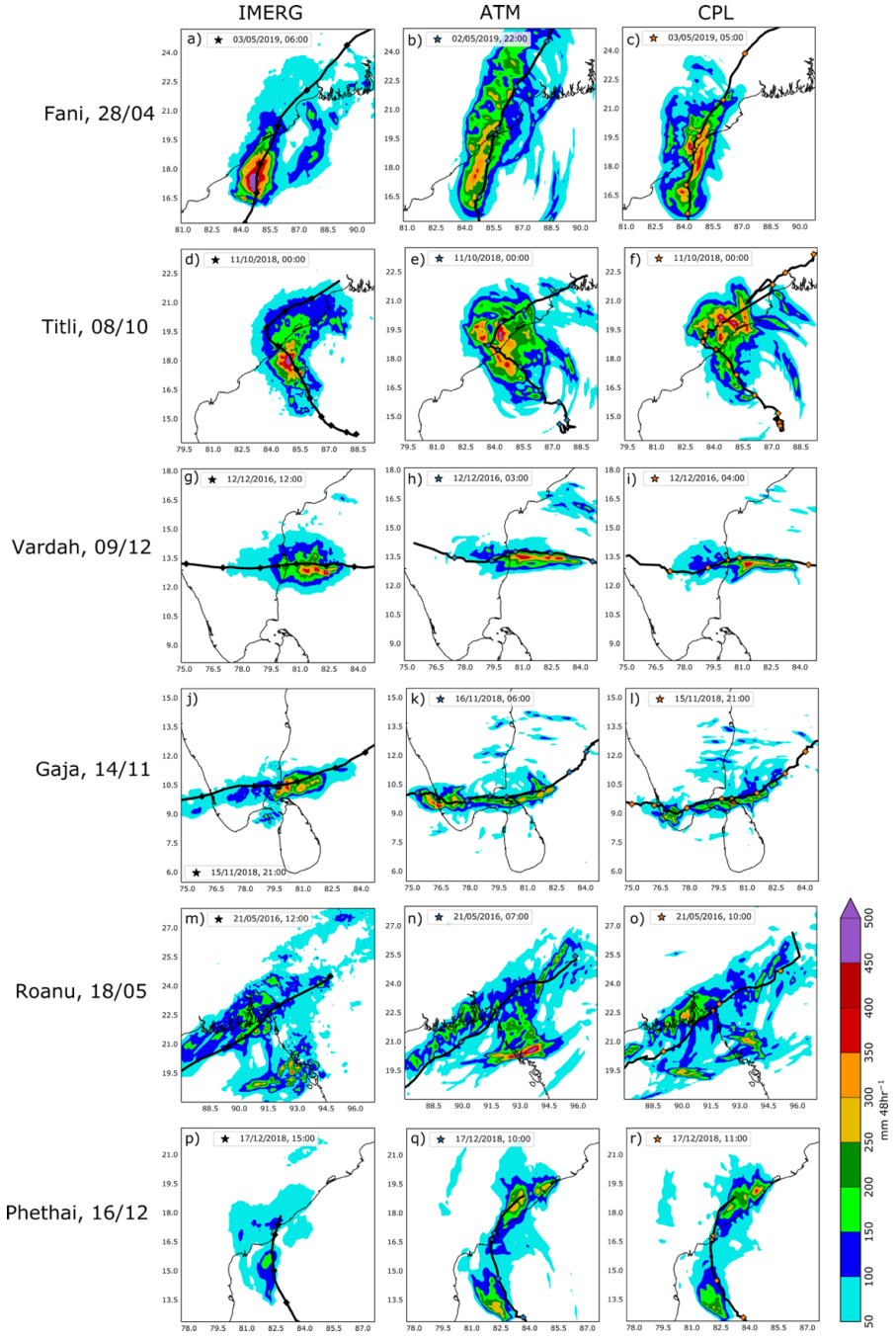

Figure 12. Accumulated rainfall from 24 hours before landfall to 24 hours after landfall in the single best-track simulation from each lagged ensemble (centre: ATM, right: CPL), within 5° of the storm centre, re-gridded to IMERG resolution (0.1° × 0.1°); and IMERG observations (left). Diamonds mark every 12 hours; stars indicate landfall time. Black lines and symbols on the IMERG plots are best track observations (IBTrACS).

https://doi.org/10.5194/wcd-2021-46
Preprint. Discussion started: 26 July 2021

5 Discussion and conclusions

This study evaluates the performance of atmosphere-only (ATM) and atmosphere-ocean coupled (CPL) configurations of the regional convective-scale IND1 model for simulating TCs over the Bay of Bengal. In each configuration, we evaluate 29 simulations of six TCs during the 2016–2019 cyclone seasons.

Of all the IND1 model simulations in this study, which are initialised up to 6 days before landfall, landfall position errors range from 15 to 409 km (mean of 130 km), if we exclude storm Roanu, for which landfall position errors are primarily due to the track of the storm closely following the coastline. Track errors over the whole TC lifetime are smaller for TCs moving from south to north than for east to west propagating systems. Both models are more skilful when initialised at higher-intensity stages of the TC lifecycle, in agreement with previous studies (e.g. Routray et al., 2017). Cyclone tracks are better in ATM than CPL for all but the strongest two TCs and better in CPL than ATM for the strongest TC. However, differences are small, which is expected as forecast motion errors are primarily driven by errors in the environmental wind field (Galarneau & Davis, 2012), which is constrained by identical lateral boundary conditions in both sets of simulations. Location and timing of landfall are more accurate for more intense storms and those moving from south to north. Excluding TC Roanu, the mean absolute landfall timing error is 13 hours (ATM) or 12 hours (CPL). For TC Roanu the errors are 83 hours (ATM) or 78 hours (CPL). For similar lead times, landfall position errors are comparable to reported errors for Vardah and Roanu forecasted using atmosphere-only configurations of WRF and the Hurricane Weather Research and Forecasting (HWRF) model (Nadimpalli et al., 2020). Position errors also compare favourably to global model simulations of TC Fani (Singh et al., 2021).

Both ATM and CPL underestimate the intensity of stronger TCs and overestimate the intensity of weaker TCs. Nadimpalli et al. (2020) have highlighted a similar bias in the WRF model for Bay of Bengal cyclones. In general, CPL predicts less intense storms than ATM, consistent with the lower SSTs and overestimation of SST cooling in cyclone wakes in CPL. Compared to IBTrACS and SYNOP observations, both models generally underestimate high wind speeds and overestimate low wind speeds. The CPL configuration gives improved pressure-wind relationships than ATM (Figure 5). However, in both configurations, there is a bias in the maximum wind speed–minimum MSLP relationship shown here (too strong MSLP/too weak wind speeds), which is also a known feature of the global atmosphere-only MetUM with parameterised convection (Heming, 2018).

For Fani, the most intense cyclone, both ATM and CPL underestimate peak intensity measured by maximum wind speed by up to ~ 35 m s^{-1} compared to IBTrACS USA data. TC Fani reaches Category 5 on the Saffir–Simpson hurricane wind scale in the observations, but a maximum of Category 3 in the models: the model fails to replicate a period of rapid intensification from 29th to 30th April 2019. In the observations, maximum wind speed is 59 m s^{-1} (Category 4) at the point of observed landfall, but in the simulations maximum wind speed is 37–45 m s^{-1} (Category 1-2) at the point of simulated landfall. The magnitude of the wind speed biases in the simulations could have significant implications for hazard predictions and subsequent warnings in any future operational implementation. It is important to note the discrepancy between maximum wind speeds in the

https://doi.org/10.5194/wcd-2021-46
Preprint. Discussion started: 26 July 2021

IBTrACS New Delhi and USA datasets. Wind speeds are generally higher in the USA data. If the New Delhi data are used, there are only small errors in maximum wind speeds at landfall for the six storms (mean error < 1 m s^{-1} when comparing forecast wind speed at forecast landfall time with observed wind speed at observed landfall time, i.e., ignoring timing errors), highlighting the uncertainty in what is 'truth'. Mean absolute errors outside the eyewall, calculated relative to SYNOP observations for the simulations with low track errors (i.e., excluding those marked with an asterisk in Table 2), are 3.6 m s^{-1} (ATM) and 3.2 m s^{-1} (CPL), with standard deviations of 3.0 and 2.8 m s^{-1}, respectively.

Theory, models and reanalysis suggest that TC potential intensity increases with SST at a rate of approximately 7.6 m s^{-1} $°C^{-1}$ (Ramsay & Sobel, 2011; Vecchi & Soden, 2007), and the predictability of TC intensity is sensitive to SST (Keshavamurthy & Kieu, 2021). TC potential intensity is linked to both regional mean SST and local SST changes, such as those associated with cold wakes caused by atmosphere-ocean feedback (Vecchi and Soden, 2007; Ramsay and Sobel, 2011; Lin et al., 2013). Cold wakes act to reduce available heat and moisture transfer from the ocean to the atmosphere under the TC centre, moderating TC intensity (Lin et al., 2013). It is consistent that the storms in CPL are weaker because CPL explicitly simulates cold ocean wakes, which in ATM are poorly timed and weaker than observed wakes. SSTs are also cold-biased throughout the model domain in CPL; however, the biases are relatively low (< 1°C) given that the ocean component is free running and only forced with assimilative global model boundaries.

In CPL, SST cold biases are stronger in cyclone wakes than the mean cold bias in the wider region. SST cooling could be overestimated if the modelled TCs were too intense or too slow. However, this does not appear to be the case here, as SST cooling is overestimated even for TCs with accurate landfall times and where intensity is underestimated in the simulations (e.g., TC Titli). Therefore, CPL overestimates the cooling response for a given TC intensity. SST cooling caused by wind-driven mixing is strongly modulated by pre-storm oceanic conditions, including mixed layer depth (Dutta et al., 2020; Vincent et al., 2012; Yesubabu et al., 2020). Analysis of a month-long period in summer 2016 has shown that coupled IND1 simulations produce a shallower mean ocean mixed layer depth (depth < ~15 m) across the Bay of Bengal in IND1 compared to FOAM (Forecast Ocean Assimilation Model) analyses and the three RAMA moorings in the Bay of Bengal. This bias is primarily due to errors in ocean initialisation (too-cold upper-ocean temperatures) and, to a lesser degree, a negative bias in net surface heat input into the ocean (Valdivieso et al., 2021). Enhanced wind-driven mixing, and the resulting entrainment of too-cold water from the thermocline associated with the TC, would lead to cold-biased SSTs in the coupled IND1 model. Sensitivity experiments where SST is artificially increased in CPL to correct the SST bias would indicate the extent to which TC intensity biases could be corrected by improving the ocean initial conditions. Coupling the atmosphere and ocean models to a wave model would also influence ocean vertical mixing, although this effect is expected to be small for the Bay of Bengal region.

In the post-monsoon TC season (late September to December), the Bay of Bengal's hydrography is not conducive to SST cooling (e.g. Chaudhuri et al., 2019). It is characterised by a shallow surface layer of freshwater from river runoff and monsoon rainfall, which caps a deep warm layer. This warm water at depth, together with salinity stratification, which reduces the depth of vertical mixing, can mean there is a near-absence

https://doi.org/10.5194/wcd-2021-46
Preprint. Discussion started: 26 July 2021

of SST cooling in the wake of even the strongest TCs post-monsoon (Chaudhuri et al., 2019; Neetu et al., 2012; Sengupta et al., 2008; Subrahmanyam et al., 2005). General circulation models have difficulty simulating the Bay of Bengal's salinity stratification (Chowdary et al., 2016). Freshwater inputs to the Bay of Bengal are not represented in the IND1 model, meaning there are salinity biases in the TC runs in this study; this is a crucial future area for model development. In contrast, in the pre-monsoon period, the warmest water is at the surface, and mixing cools SST (Krishna et al., 1993; Kumar et al., 2019), meaning TC-induced cooling is three times larger in the pre-monsoon season (Neetu et al., 2012). These differences in pre- and post-monsoon ocean conditions could explain why CPL overestimates cooling in the storm wake for the four post-monsoon storms in this study (Titli, Vardah, Gaja and Phethai) but has smaller negative biases in the wake compared to the wider region for the two pre-monsoon storms (Fani and Roanu). The SST cooling simulated in the CPL simulations after the passage of tropical storm Roanu (up to ~ 2°C) is a good match to data from a custom-made Lagrangian float and Argo floats from Kumar et al. (2019), which show that almost the entire Bay of Bengal north of 12°N cooled by 1–2 °C during the passage of the storm, with ~ 50% of this cooling attributed to wind-driven mixing.

While SST cooling in the wake of the post-monsoon storms is too strong in CPL, it is not sufficiently strong in ATM, indicated by larger warm biases in the cyclone wakes than the rest of the domain. This could be partly due to the lag between the time of observations contributing to OSTIA data and the validity time at which it is applied in the simulations. A time lag of one day is significant given the short timescales of SST change associated with TC intensification and cold wakes (hours to days; Price, 1981). The warm-biased TC wakes in ATM could indicate that the cooling feature in OSTIA occurs after the end of the simulations. Also, comparisons of OSTIA observations to moored buoys have shown that cyclone cold wakes can be poorly captured in OSTIA (Liu et al., 2018) due to the difficulty in obtaining accurate satellite SST measurements through thick clouds such as those associated with cyclones (Sunder et al., 2020).

TC simulations are sensitive to initial SST conditions, as well as coupling (Feng et al., 2019). This means that the negative intensity biases in CPL could be due to cold-biased initial SSTs, in addition to an overestimation of cooling in cyclone wakes. In fact, coupling alone cannot explain the intensity biases in this study, as we find no relationship between SST biases in the storm wake and intensity biases (not shown). However, it is challenging to observe storm wake bias directly under the eyewall, where cooling would most impact intensity. To determine the relative impacts of coupling and initial SST on cyclone intensity requires SST sensitivity experiments where ATM and CPL are run with the same ocean initial conditions, and ATM SSTs are updated with the output of standalone ocean runs so that SSTs in the ATM and CPL runs are equivalent apart from air–sea feedbacks.

High rain rates are underestimated in both configurations relative to IMERG, while low rain rates are overestimated. Compared to IMERG observations, both models produce good predictions for the magnitude of rainfall associated with landfalling TCs. Inner rain rate is slightly underestimated over the ocean but overestimated after landfall. It is important to note here that differences between IMERG and other satellite datasets have been found to vary with the surface type (land or ocean; Liu, 2016). Moreover, comparisons to rain gauges have shown that IMERG is less accurate at higher altitudes (Xu et al., 2017), so caution should be

https://doi.org/10.5194/wcd-2021-46
Preprint. Discussion started: 26 July 2021

exercised when interpreting biases relative to IMERG after landfall when the storms all move over higher-altitude regions. In general, CPL has lower rain rates than ATM and lower accumulated rainfall for 48 hours around landfall. Rain rates are much higher for more intense storms in the simulations, but not in IMERG, which is consistent with studies showing that maximum rainfall in IMERG is not related to TC intensity in IBTrACS for TCs in the Bay of Bengal (Thakur et al., 2018) and China (Yu et al., 2017). In addition to intensity, rainfall bias in the simulations may be associated with large-scale SST biases, which affect moisture availability and vertical instability; therefore, the lower rain rates in CPL could be due to the cold-biased SSTs in the CPL configuration, which originate from the ocean initialisation. This relationship could be investigated using the same SST sensitivity experiments described above, where SST in the ATM model is artificially increased or decreased. Both models produce reasonable predictions of the location of rainfall associated with landfalling TCs. Maximum rain rates are generally observed to the left of the cyclone track before landfall, typical for Bay of Bengal TCs (Ankur et al., 2020) and monsoon depressions (Hunt et al., 2016); this is well captured in the models. The simulations predict more spiral rainbands than IMERG.

Both ATM and CPL produce accurate predictions for rain rate asymmetry, with little difference between models, suggesting a good representation of TC dynamics in the model configurations. Much of the variation in rain rate asymmetry, in both the simulations and observations, can be explained by variations in wind shear with higher rain rates in the down-shear left quadrant (Alvey III et al., 2015; Chen et al., 2006; DeHart et al., 2014; Xu et al., 2014; Yu et al., 2017). Wind shear cannot explain all the rainfall asymmetry variation in the simulations or all the discrepancies between the simulations and IMERG.

In operational forecasts, simulations of TC track, landfall time, landfall location and intensity are essential in planning mitigation efforts. In this study, the IND1 regional model is driven at the boundaries by the global MetUM, which is re-initialised every day from the MetUM global analysis, a procedure that cannot be applied operationally. Using a truly free-running atmospheric forecast to provide lateral boundary conditions is likely to degrade forecast performance relative to that shown in this study, and would be of value in future assessments of the IND1 system.. In addition, most operational atmosphere-only TC simulations use persisted SST throughout the model run (e.g. Routray et al., 2017) in contrast to the daily updating SST data used in this study. Previous studies suggest that the biases in ATM might deteriorate if SST were instead persisted throughout model runs: Rai et al. (2019) conducted simulations of TC Phailin (October 2013, Bay of Bengal) with persisted and daily updating SST. Using the daily updating SST improved storm track and intensity estimates by 37% and 41%, respectively. Mohanty et al. (2019) determined that the impact of updating simulations with realistic SSTs during TC lifetimes improved landfall position and timing predictions by 20% and 33%, respectively. With a lack of data assimilation in the oceanic component, the CPL configuration performs well relative to ATM, given the observed SST used in ATM.

This study has found that the convection-permitting regional IND1 model, in both an atmosphere-only and a coupled configuration, can accurately simulate the track, intensity, and structure of tropical cyclones in the Bay of Bengal. The model generally underestimates high wind speeds and high rain rates and overestimates low wind speeds and low rain rates. The track errors are generally slightly lower in ATM, but minimum MSLP

https://doi.org/10.5194/wcd-2021-46
Preprint. Discussion started: 26 July 2021

absolute errors are generally slightly lower in CPL, and for several storms, CPL has slightly lower maximum wind absolute errors. The similarity between ATM and CPL indicates that many of the deficiencies in the simulations originate in the atmospheric model. Future areas for model improvement include reducing the intensity biases (or applying bias-correction methods) and improving the representation of rapid intensification for the most intense cyclones. Development of the CPL configuration should include an adjustment of ocean initial and boundary conditions, as SST throughout the model domain is too cold. Future refinements could also be made to the regional ocean dynamics and vertical structure, including coupling the present configuration to a wave model, as CPL overestimates cooling in TC wakes. Any candidate operational implementation would require further evaluation to determine the impact of lateral atmospheric boundary conditions obtained from free-running forecasts, ideally from a global coupled model, and for the ATM configuration, the impact of persisting SST throughout model runs. Coupled systems provide a physically sound approach to introducing air–sea interactions, which are important for track and intensity predictions, to tropical cyclone forecasts. However, there are outstanding challenges related to ocean dynamics in both the coupled system development and model initialisation.

Code/data availability. The model code and raw data were generated at the Met Office. The data that support the findings of this study are available from the corresponding author, J Saxby, upon reasonable request.

Author contribution. Huw Lewis and Juan Castillo implemented the IND1 system, designed the simulations and Juan Castillo carried them out. Project administration and data curation was carried out by Nicholas Klingaman, Chris Holloway, Huw Lewis and Juliane Schwendike. Funding acquisition by Nicholas Klingaman, Chris Holloway, Maria Valdivieso da Costa, Juliane Schwendike, Cathryn Birch and Simon Peatman. Formal analysis and data visualisation was carried out by Jennifer Saxby and Julia Crook. Jennifer Saxby and Julia Crook prepared the manuscript with contributions from all co-authors. All co-authors helped guide the analysis and reviewed and edited the manuscript.

Competing interests. The authors declare that they have no conflict of interest.

Acknowledgements. This work and its authors were supported by the Weather and Climate Science for Service Partnership (WCSSP) India, a collaborative initiative between the Met Office, supported by the UK Government's Newton Fund, and the Indian Ministry of Earth Sciences (MoES). This work is part of the Coupled Air-Sea Prediction of Extreme Rainfall (CASPER) project. NPK was also supported by an Independent Research Fellowship from the Natural Environment Research Council (NE/L010976/1) and by the ACREW programme of the National Centre for Atmospheric Science, under the UK Global Challenges Research Fund. The authors thank John Ashcroft (University of Leeds) for providing the tropical cyclone tracking code and his valuable assistance with developing this, and Kevin Hodges (University of Reading) for sharing output from his TRACK algorithm run on reanalysis and simulations of TC Fani. This work used JASMIN, the UK's collaborative data analysis environment (http://jasmin.ac.uk). The International Best Track Archive for Climate Stewardship (IBTrACS) data were developed by NOAA's National Climatic Data Center. ERA5 data were downloaded from the Copernicus Climate Data Store (CDS); neither the European Commission nor ECMWF is

https://doi.org/10.5194/wcd-2021-46
Preprint. Discussion started: 26 July 2021

responsible for this use of the Copernicus data. We are grateful to the GTMBA Project Office of NOAA/PMEL for the use of RAMA buoy data. Argo float data were collected and made freely available by the International Argo Program and the national programs that contribute to it (https://argo.ucsd.edu, https://www.ocean-ops.org). The Argo Program is part of the Global Ocean Observing System. We are grateful to the Centre for Environmental Data Analysis, the NCAS British Atmospheric Data Centre and the Met Office for access to SYNOP data through the MetDB service. IMERG data were provided by NASA and PPS, which develop and compute IMERG as a contribution to GPM, which are archived at the NASA GES DISC.

References.

Agrawal, N., Pandey, V. K., & Kumar, P. (2020). Numerical Simulation of Tropical Cyclone Mora Using a Regional Coupled Ocean-Atmospheric Model. *Pure and Applied Geophysics*, *177*(11), 5507–5521. https://doi.org/10.1007/s00024-020-02563-4

Ali, A. (1999). Climate change impacts and adaptation assessment in Bangladesh. *Climate Research*, *12*(2–3), 109–116. https://doi.org/10.3354/cr012109

Alley, R. B., Emanuel, K. A., & Zhang, F. (2019). Advances in weather prediction. *Science*, *363*(6425), 342–344. https://doi.org/10.1126/science.aav7274

Alvey III, G. R., Zawislak, J., & Zipser, E. (2015). Precipitation Properties Observed during Tropical Cyclone Intensity Change. *Monthly Weather Review*, *143*(11), 4476–4492. https://doi.org/10.1175/MWR-D-15-0065.1

Anandh, T. S., Das, B. K., Kuttippurath, J., & Chakraborty, A. (2020). A coupled model analyses on the interaction between oceanic eddies and tropical cyclones over the Bay of Bengal. *Ocean Dynamics*, *70*(3), 327–337. https://doi.org/10.1007/s10236-019-01330-x

Ankur, K., Busireddy, N. K. R., Osuri, K. K., & Niyogi, D. (2020). On the relationship between intensity changes and rainfall distribution in tropical cyclones over the North Indian Ocean. *International Journal of Climatology*, *40*(4), 2015–2025. https://doi.org/10.1002/joc.6315

Argo (2020). Argo float data and metadata from Global Data Assembly Centre (Argo GDAC). SEANOE. https://doi.org/10.17882/42182

Baisya, H., Pattnaik, S., & Chakraborty, T. (2020). A coupled modeling approach to understand ocean coupling and energetics of tropical cyclones in the Bay of Bengal basin. *Atmospheric Research*, *246*, 105092. https://doi.org/10.1016/j.atmosres.2020.105092

Balaguru, K., Taraphdar, S., Leung, L. R., & Foltz, G. R. (2014). Increase in the intensity of postmonsoon Bay of Bengal tropical cyclones. *Geophysical Research Letters*, *41*(10), 3594–3601. https://doi.org/10.1002/2014GL060197

Bandyopadhyay, S., Dasgupta, Susmita, Khan, Z. H., & Wheeler, D. (2018). *Cyclonic Storm Landfalls in Bangladesh, West Bengal and Odisha, 1877-2016: A Spatiotemporal Analysis*. https://elibrary.worldbank.org/doi/book/10.1596/1813-9450-8316

Bender, M. A., & Ginis, I. (2000). Real-Case Simulations of Hurricane–Ocean Interaction Using A High-Resolution Coupled Model: Effects on Hurricane Intensity. *Monthly Weather Review*, *128*, 30.

Bender, M. A., Ginis, I., & Kurihara, Y. (1993). Numerical simulations of tropical cyclone-ocean interaction with a high-resolution coupled model. *Journal of Geophysical Research: Atmospheres*, *98*(D12), 23245–23263. https://doi.org/10.1029/93JD02370

Best, M. J., Pryor, M., Clark, D. B., Rooney, G. G., Essery, R. L. H., Ménard, C. B., Edwards, J. M., Hendry, M. A., Porson, A., Gedney, N., Mercado, L. M., Sitch, S., Blyth, E., Boucher, O., Cox, P. M., Grimmond, C. S. B., & Harding, R. J. (2011). The Joint UK Land Environment Simulator (JULES), model description – Part 1: Energy and water fluxes. *Geoscientific Model Development*, *4*(3), 677–699. https://doi.org/10.5194/gmd-4-677-2011

Biswas, M. K., Abarca, S., Bernardet, L., Ginis, I., Grell, E., Iacono, M., Kalina, E., Liu, B., Liu, Q., Marchok, T., Mehra, A., Newman, K., Sippel, J., Tallapragada, V., Thomas, B., Wang, W., Winterbottom, H., & Zhang, Z. (2018). *Hurricane Weather Research and Forecasting (HWRF) Model: 2018 Scientific Documentation*. Developmental Testbed Center.

https://doi.org/10.5194/wcd-2021-46
Preprint. Discussion started: 26 July 2021

Brown, A., Milton, S., Cullen, M., Golding, B., Mitchell, J., & Shelly, A. (2012). Unified Modeling and Prediction of Weather and Climate: A 25-Year Journey. *Bulletin of the American Meteorological Society*, *93*(12), 1865–1877. https://doi.org/10.1175/BAMS-D-12-00018.1

Bush, M., Allen, T., Bain, C., Boutle, I., Edwards, J., Finnenkoetter, A., Franklin, C., Hanley, K., Lean, H., Lock, A., Manners, J., Mittermaier, M., Morcrette, C., North, R., Petch, J., Short, C., Vosper, S., Walters, D., Webster, S., Weeks, M., Wilkinson, J., Wood, N., & Zerroukat, M. (2020). The first Met Office Unified Model–JULES Regional Atmosphere and Land configuration, RAL1, *Geoscientific Model Development*, 13, 1999–2029, https://doi.org/10.5194/gmd-13-1999-2020

Castillo, J., Lewis, H. et al. (in prep). The IND1 regional environmental prediction coupled modelling framework.

Chan, J. C. L. (2005). The physics of tropical cyclone motion. *Annual Review of Fluid Mechanics*, *37*(1), 99–128. https://doi.org/10.1146/annurev.fluid.37.061903.175702

Chan, J. C. L., & Liang, X. (2003). Convective Asymmetries Associated with Tropical Cyclone Landfall. Part I: F-Plane Simulations. *Journal of the Atmospheric Sciences*, *60*(13), 1560–1576. https://doi.org/10.1175/1520-0469(2003)60<1560:CAAWTC>2.0.CO;2

Chaudhuri, D., Sengupta, D., D'Asaro, E., Venkatesan, R., & Ravichandran, M. (2019). Response of the Salinity-Stratified Bay of Bengal to Cyclone Phailin. *Journal of Physical Oceanography*, *49*(5), 1121–1140. https://doi.org/10.1175/JPO-D-18-0051.1

Chen, S. S., Knaff, J. A., & Marks, F. D. (2006). Effects of Vertical Wind Shear and Storm Motion on Tropical Cyclone Rainfall Asymmetries Deduced from TRMM. *Monthly Weather Review*, *134*(11), 3190–3208. https://doi.org/10.1175/MWR3245.1

Chen, S. S., Price, J. F., Zhao, W., Donelan, M. A., & Walsh, E. J. (2007). The CBLAST-Hurricane Program and the Next-Generation Fully Coupled Atmosphere–Wave–Ocean Models for Hurricane Research and Prediction. *Bulletin of the American Meteorological Society*, *88*(3), 311–318. https://doi.org/10.1175/BAMS-88-3-311

Chowdary, J., Srinivas, G., Fousiya, T. S., Parekh, A., Gnanaseelan, C., Seo, H., & MacKinnon, J. (2016). Representation of Bay of Bengal Upper-Ocean Salinity in General Circulation Models. *Oceanography*, *29*(2), 38–49. https://doi.org/10.5670/oceanog.2016.37

Clark, D. B., Mercado, L. M., Sitch, S., Jones, C. D., Gedney, N., Best, M. J., Pryor, M., Rooney, G. G., Essery, R. L. H., Blyth, E., Boucher, O., Harding, R. J., Huntingford, C., & Cox, P. M. (2011). The Joint UK Land Environment Simulator (JULES), model description – Part 2: Carbon fluxes and vegetation dynamics. *Geoscientific Model Development*, *4*(3), 701–722. https://doi.org/10.5194/gmd-4-701-2011

Corbosiero, K. L., & Molinari, J. (2003). The Relationship between Storm Motion, Vertical Wind Shear, and Convective Asymmetries in Tropical Cyclones. *Journal of the Atmospheric Sciences*, *60*(2), 366–376. https://doi.org/10.1175/1520-0469(2003)060<0366:TRBSMV>2.0.CO;2

Dasgupta, S., Huq, M., Khan, Z. H., Ahmed, M. M. Z., Mukherjee, N., Khan, M. F., & Pandey, K. (2014). Cyclones in a changing climate: The case of Bangladesh. *Climate and Development*, *6*(2), 96–110. https://doi.org/10.1080/17565529.2013.868335

DeHart, J. C., Houze, R. A., & Rogers, R. F. (2014). Quadrant Distribution of Tropical Cyclone Inner-Core Kinematics in Relation to Environmental Shear. *Journal of the Atmospheric Sciences*, *71*(7), 2713–2732. https://doi.org/10.1175/JAS-D-13-0298.1

DeMaria, M., Sampson, C. R., Knaff, J. A., & Musgrave, K. D. (2013). Is Tropical Cyclone Intensity Guidance Improving? *Bulletin of the American Meteorological Society*, *95*(3), 387–398. https://doi.org/10.1175/BAMS-D-12-00240.1

Deng, D., & Ritchie, E. A. (2018). Rainfall Characteristics of Recurving Tropical Cyclones over the Western North Pacific. *Journal of Climate*, *31*(2), 575–592. https://doi.org/10.1175/JCLI-D-17-0415.1

Donlon, C. J., Martin, M., Stark, J., Roberts-Jones, J., Fiedler, E., & Wimmer, W. (2012). The Operational Sea Surface Temperature and Sea Ice Analysis (OSTIA) system. *Remote Sensing of Environment*, *116*, 140–158. https://doi.org/10.1016/j.rse.2010.10.017

Dutta, D., Mani, B., & Dash, M. K. (2020). Dynamic and thermodynamic upper-ocean response to the passage of Bay of Bengal cyclones 'Phailin' and 'Hudhud': A study using a coupled modelling system. *Environmental Monitoring and Assessment*, *191*(3), 808. https://doi.org/10.1007/s10661-019-7704-9

https://doi.org/10.5194/wcd-2021-46
Preprint. Discussion started: 26 July 2021

Emanuel, K. A. (1999). Thermodynamic control of hurricane intensity. *Nature*, *401*(6754), 665–669. https://doi.org/10.1038/44326

Feng, X., Klingaman, N. P., & Hodges, K. I. (2019). The effect of atmosphere–ocean coupling on the prediction of 2016 western North Pacific tropical cyclones. *Quarterly Journal of the Royal Meteorological Society*, *145*(723), 2425–2444. https://doi.org/10.1002/qj.3571

Fierro, A. O., Rogers, R. F., Marks, F. D., & Nolan, D. S. (2009). The Impact of Horizontal Grid Spacing on the Microphysical and Kinematic Structures of Strong Tropical Cyclones Simulated with the WRF-ARW Model. *Monthly Weather Review*, *137*(11), 3717–3743. https://doi.org/10.1175/2009MWR2946.1

Frank, W. M., & Ritchie, E. A. (1999). Effects of Environmental Flow upon Tropical Cyclone Structure. *Monthly Weather Review*, *127*, 18.

Galarneau, T. J., & Davis, C. A. (2012). Diagnosing Forecast Errors in Tropical Cyclone Motion. *Monthly Weather Review*, *141*(2), 405–430. https://doi.org/10.1175/MWR-D-12-00071.1

Gopalakrishnan, S. G., Goldenberg, S., Quirino, T., Zhang, X., Marks, F., Yeh, K.-S., Atlas, R., & Tallapragada, V. (2012). Toward Improving High-Resolution Numerical Hurricane Forecasting: Influence of Model Horizontal Grid Resolution, Initialization, and Physics. *Weather and Forecasting*, *27*(3), 647–666. https://doi.org/10.1175/WAF-D-11-00055.1

Greeshma, M., Srinivas, C. V., Prasad, K. B. R. R. H., Baskaran, R., & Venkatraman, B. (2019). Sensitivity of tropical cyclone predictions in the coupled atmosphere–ocean model WRF-3DPWP to surface roughness schemes. *Meteorological Applications*, *26*(2), 324–346. https://doi.org/10.1002/met.1765

Hart, R. E. (2003). A Cyclone Phase Space Derived from Thermal Wind and Thermal Asymmetry. *Monthly Weather Review*, *131*(4), 585–616. https://doi.org/10.1175/1520-0493(2003)131<0585:ACPSDF>2.0.CO;2

Heming, J. T. (2016). Met Office Unified Model Tropical Cyclone Performance Following Major Changes to the Initialization Scheme and a Model Upgrade. *Weather and Forecasting*, *31*(5), 1433–1449. https://doi.org/10.1175/WAF-D-16-0040.1

Heming, J. T. (2018, April 18). *The Impact of Recently Implemented and Planned Changes to the Met Office Global Model on Tropical Cyclone Performance*. 33rd Conference on Hurricanes and Tropical Meteorology. https://ams.confex.com/ams/33HURRICANE/webprogram/Paper339027.html

Hence, D. A., & Houze, R. A. (2012). Vertical Structure of Tropical Cyclone Rainbands as Seen by the TRMM Precipitation Radar. *Journal of the Atmospheric Sciences*, *69*(9), 2644–2661. https://doi.org/10.1175/JAS-D-11-0323.1

Hersbach, H., Bell, B., Berrisford, P., Biavati, G., Horányi, A., Muñoz Sabater, J., Nicolas, J.,Peubey, C., Radu, R., Rozum, I., Schepers, D., Simmons, A., Soci, C., Dee, D., Thépaut, J-N. (2018a): ERA5 hourly data on single levels from 1979 to present. Copernicus Climate Change Service (C3S) Climate Data Store (CDS). (Accessed on 18-DEC-2020). https://doi.org/10.24381/cds.adbb2d47

Hersbach, H., Bell, B., Berrisford, P., Biavati, G., Horányi, A., Muñoz Sabater, J., Nicolas, J.,Peubey, C., Radu, R., Rozum, I., Schepers, D., Simmons, A., Soci, C., Dee, D., Thépaut, J-N. (2018b): ERA5 hourly data on pressure levels from 1979 to present. Copernicus Climate Change Service (C3S) Climate Data Store (CDS). (Accessed on 18-DEC-2020). https://doi.org/10.24381/cds.bd0915c6

Hersbach, H., Bell, B., Berrisford, P., Hirahara, S., Horányi, A., Muñoz-Sabater, J., Nicolas, J., Peubey, C., Radu, R., Schepers, D., Simmons, A., Soci, C., Abdalla, S., Abellan, X., Balsamo, G., Bechtold, P., Biavati, G., Bidlot, J., Bonavita, M., … Thépaut, J.-N. (2020). The ERA5 global reanalysis. *Quarterly Journal of the Royal Meteorological Society*, *146*(730), 1999–2049. https://doi.org/10.1002/qj.3803

Hirahara, S., Alonso-Balmaseda, M., de Boisseson, E., & Hersbach, H. (2016). *Sea Surface Temperature and Sea Ice Concentration for ERA5*. ECMWF.

Hodges, K. I. (1995). Feature tracking on the unit sphere. *Monthly Weather Review*, *123*(12), 3458–3465. https://doi.org/10.1175/1520-0493(1995)123<3458:FTOTUS>2.0.CO;2

Hodges, K. I., & Klingaman, N. P. (2019). Prediction Errors of Tropical Cyclones in the Western North Pacific in the Met Office Global Forecast Model. *Weather and Forecasting*, *34*(5), 1189–1209. https://doi.org/10.1175/WAF-D-19-0005.1

https://doi.org/10.5194/wcd-2021-46
Preprint. Discussion started: 26 July 2021

Huffman, G. J., Bolvin, D.T., Braithwaite, D., Hsu, K.-L., Joyce, R.J., & Xie, P. (2014). Integrated Multi-satellitE Retrievals for GPM (IMERG), version 4.4. NASA's Precipitation Processing Center, accessed [01-SEP-2019]. ftp://arthurhou.pps.eosdis.nasa.gov/gpmdata/

Huffman, G. J., Bolvin, D. T., Braithwaite, D., Hsu, K.-L., Joyce, R. J., Kidd, C., Nelkin, E. J., Sorooshian, S., Stocker, E. F., Tan, J., Wolff, D. B., & Xie, P. (2020). Integrated Multi-satellite Retrievals for the Global Precipitation Measurement (GPM) Mission (IMERG). In V. Levizzani, C. Kidd, D. B. Kirschbaum, C. D. Kummerow, K. Nakamura, & F. J. Turk (Eds.), *Satellite Precipitation Measurement: Volume 1* (pp. 343–353). Springer International Publishing. https://doi.org/10.1007/978-3-030-24568-9_19

Hunt, K. M. R., Turner, A. G., & Parker, D. E. (2016). The spatiotemporal structure of precipitation in Indian monsoon depressions. *Quarterly Journal of the Royal Meteorological Society*, *142*(701), 3195–3210. https://doi.org/10.1002/qj.2901

Jin, H., Peng, M. S., Jin, Y., & Doyle, J. D. (2013). An Evaluation of the Impact of Horizontal Resolution on Tropical Cyclone Predictions Using COAMPS-TC. *Weather and Forecasting*, *29*(2), 252–270. https://doi.org/10.1175/WAF-D-13-00054.1

Keshavamurthy, K., & Kieu, C. (2021). Dependence of tropical cyclone intrinsic intensity variability on the large-scale environment. *Quarterly Journal of the Royal Meteorological Society*, *147*(736), 1606–1625. https://doi.org/10.1002/qj.3984

Khain, A., & Ginis, I. (1991). The mutual response of a moving tropical cyclone and the ocean. *Beiträge zur Physik der Atmosphäre, 64*, 125-141.

Knapp, K. R., Kruk, M. C., Levinson, D. H., Diamond, H. J., & Neumann, C. J. (2010). The International Best Track Archive for Climate Stewardship (IBTrACS): Unifying Tropical Cyclone Data. *Bulletin of the American Meteorological Society*, *91*(3), 363–376. https://doi.org/10.1175/2009BAMS2755.1

Knapp, K. R., Diamond, H. J., Kossin, J. P., Kruk, M. C. & Schreck, C. J. III (2018). International Best Track Archive for Climate Stewardship (IBTrACS) Project, Version 4. [2016-2019]. NOAA National Centers for Environmental Information. https://doi.org/10.25921/82ty-9e16 [28-JAN-2020].

Krishna, V. V. G., Murty, V. S. N., Sarma, M. S. S., & Sastry, J. S. (1993). Thermal response of upper layers of Bay of Bengal to forcing of a severe cyclonic storm: A case study. *IJMS, 22*(1). http://nopr.niscair.res.in/handle/123456789/37744

Kumar, B. P., D'Asaro, E., Suresh Kumar, N., & Ravichandran, M. (2019). Widespread cooling of the Bay of Bengal by tropical storm Roanu. *Deep Sea Research Part II: Topical Studies in Oceanography*, *168*, 104652. https://doi.org/10.1016/j.dsr2.2019.104652

Lewis, H. W., Castillo Sanchez, J. M., Arnold, A., Fallmann, J., Saulter, A., Graham, J., Bush, M., Siddorn, J., Palmer, T., Lock, A., Edwards, J., Bricheno, L., Martínez-de la Torre, A., & Clark, J. (2019). The UKC3 regional coupled environmental prediction system. *Geoscientific Model Development*, *12*(6), 2357–2400. https://doi.org/10.5194/gmd-12-2357-2019

Lin, I.-I., Black, P., Price, J. F., Yang, C.-Y., Chen, S. S., Lien, C.-C., Harr, P., Chi, N.-H., Wu, C.-C., & D'Asaro, E. A. (2013). An ocean coupling potential intensity index for tropical cyclones. *Geophysical Research Letters*, *40*(9), 1878–1882. https://doi.org/10.1002/grl.50091

Liu, Y., Weisberg, R. H., Law, J., & Huang, B. (2018). Evaluation of Satellite-Derived SST Products in Identifying the Rapid Temperature Drop on the West Florida Shelf Associated With Hurricane Irma. *Marine Technology Society Journal*, *52*(3), 43–50. https://doi.org/10.4031/MTSJ.52.3.7

Liu, Z. (2016). Comparison of Integrated Multisatellite Retrievals for GPM (IMERG) and TRMM Multisatellite Precipitation Analysis (TMPA) Monthly Precipitation Products: Initial Results. *Journal of Hydrometeorology*, *17*(3), 777–790. https://doi.org/10.1175/JHM-D-15-0068.1

Gurvan, M., Bourdallé-Badie, R., Chanut, J., Clementi, E., Coward, A., Ethé, C., Iovino, D., Lea, D., Lévy, C., Lovato, T., Martin, N., Masson, S., Mocavero, S., Rousset, C., Storkey, D., Vancoppenolle, M., Müeller, S., Nurser, G., Bell, M., & Samson, G. (2019). *NEMO ocean engine*. https://doi.org/10.5281/zenodo.3878122

Mahmood, S., Lewis, H., Arnold, A., Harris, C. (2021). The impact of time varying sea surface temperature on UK regional atmosphere forecasts. *Meteorological Applications, in press.* https://doi.org/10.1002/met.1983

Mandal, M., Mohanty, U. C., Sinha, P., & Ali, M. M. (2007). Impact of sea surface temperature in modulating movement and intensity of tropical cyclones. *Natural Hazards*, *41*(3), 413–427. https://doi.org/10.1007/s11069-006-9051-8

https://doi.org/10.5194/wcd-2021-46
Preprint. Discussion started: 26 July 2021

McPhaden, M. J., Meyers, G., Ando, K., Masumoto, Y., Murty, V. S. N., Ravichandran, M., Syamsudin, F., Vialard, J., Yu, L., & Yu, W. (2009). RAMA: The Research Moored Array for African–Asian–Australian Monsoon Analysis and Prediction*. *Bulletin of the American Meteorological Society*, *90*(4), 459–480. https://doi.org/10.1175/2008BAMS2608.1

Met Office (2008a). LAND SYNOP reports from land stations collected by the Met Office MetDB System. NCAS British Atmospheric Data Centre. https://catalogue.ceda.ac.uk/uuid/9f80d42106ba708f92ada730ba321831

Met Office (2008b). SHIP SYNOP reports from ship, buoy and fixed platform stations collected by the Met Office MetDB System. NCAS British Atmospheric Data Centre. https://catalogue.ceda.ac.uk/uuid/65ca7898647cc3686492bcb8bb483a1c

Mishra, A. (2014). Temperature Rise and Trend of Cyclones over the Eastern Coastal Region of India. *Journal of Earth Science & Climatic Change*, *5*(9), 1–5. https://doi.org/10.4172/2157-7617.1000227

Mogensen, K. S., Magnusson, L., & Bidlot, J.-R. (2017). Tropical cyclone sensitivity to ocean coupling in the ECMWF coupled model. *Journal of Geophysical Research: Oceans*, *122*(5), 4392–4412. https://doi.org/10.1002/2017JC012753@10.1002/(ISSN)2169-9291.ORFTC1

Mohanty, S., Nadimpalli, R., Osuri, K. K., Pattanayak, S., Mohanty, U. C., & Sil, S. (2019). Role of Sea Surface Temperature in Modulating Life Cycle of Tropical Cyclones over Bay of Bengal. *Tropical Cyclone Research and Review*, *8*(2), 68–83. https://doi.org/10.1016/j.tcrr.2019.07.007

Mohanty, U. C., Osuri, K. K., Tallapragada, V., Marks, F. D., Pattanayak, S., Mohapatra, M., Rathore, L. S., Gopalakrishnan, S. G., & Niyogi, D. (2015). A Great Escape from the Bay of Bengal "Super Sapphire–Phailin" Tropical Cyclone: A Case of Improved Weather Forecast and Societal Response for Disaster Mitigation. *Earth Interactions*, *19*(17), 1–11. https://doi.org/10.1175/EI-D-14-0032.1

Nadimpalli, R., Osuri, K. K., Mohanty, U. C., Das, A. K., Kumar, A., Sil, S., & Niyogi, D. (2020). Forecasting tropical cyclones in the Bay of Bengal using quasi-operational WRF and HWRF modeling systems: An assessment study. *Meteorology and Atmospheric Physics*, *132*(1), 1–17. https://doi.org/10.1007/s00703-019-00669-6

Neetu, S., Lengaigne, M., Vialard, J., Samson, G., Masson, S., Krishnamohan, K. S., & Suresh, I. (2019). Premonsoon/Postmonsoon Bay of Bengal Tropical Cyclones Intensity: Role of Air-Sea Coupling and Large-Scale Background State. *Geophysical Research Letters*, *46*(4), 2149–2157. https://doi.org/10.1029/2018GL081132

Neetu, S., Lengaigne, M., Vincent, E. M., Vialard, J., Madec, G., Samson, G., Kumar, M. R. R., & Durand, F. (2012). Influence of upper-ocean stratification on tropical cyclone-induced surface cooling in the Bay of Bengal. *Journal of Geophysical Research: Oceans*, *117*(C12). https://doi.org/10.1029/2012JC008433

Nguyen, L. T., Molinari, J., & Thomas, D. (2014). Evaluation of Tropical Cyclone Center Identification Methods in Numerical Models. *Monthly Weather Review*, *142*(11), 4326–4339. https://doi.org/10.1175/MWR-D-14-00044.1

Osuri, K. K., Nadimpalli, R., Mohanty, U. C., & Niyogi, D. (2017). Prediction of rapid intensification of tropical cyclone Phailin over the Bay of Bengal using the HWRF modelling system. *Quarterly Journal of the Royal Meteorological Society*, *143*(703), 678–690. https://doi.org/10.1002/qj.2956

Pothapakula, P. K., Osuri, K. K., Pattanayak, S., Mohanty, U. C., Sil, S., & Nadimpalli, R. (2017). Observational perspective of SST changes during life cycle of tropical cyclones over Bay of Bengal. *Natural Hazards*, *88*(3), 1769–1787. https://doi.org/10.1007/s11069-017-2945-9

Prakash, K. R., & Pant, V. (2017). Upper oceanic response to tropical cyclone Phailin in the Bay of Bengal using a coupled atmosphere-ocean model. *Ocean Dynamics*, *67*(1), 51–64. https://doi.org/10.1007/s10236-016-1020-5

Price, J. F. (1981). Upper Ocean Response to a Hurricane. *Journal of Physical Oceanography*, *11*(2), 153–175. https://doi.org/10.1175/1520-0485(1981)011<0153:UORTAH>2.0.CO;2

Rai, D., Pattnaik, S., Rajesh, P. V., & Hazra, V. (2019). Impact of high resolution sea surface temperature on tropical cyclone characteristics over the Bay of Bengal using model simulations. *Meteorological Applications*, *26*(1), 130–139. https://doi.org/10.1002/met.1747

https://doi.org/10.5194/wcd-2021-46
Preprint. Discussion started: 26 July 2021

Ramsay, H. A., & Sobel, A. H. (2011). Effects of Relative and Absolute Sea Surface Temperature on Tropical Cyclone Potential Intensity Using a Single-Column Model. *Journal of Climate*, *24*(1), 183–193. https://doi.org/10.1175/2010JCLI3690.1

Rao, D. B., Naidu, C., & Rao, B. S. (2001). Trends and fluctuations of the cyclonic systems over North Indian Ocean. *Mausam*, *52*(1), 37–46.

Routray, A., Singh, V., George, J. P., Mohandas, S., & Rajagopal, E. N. (2017). Simulation of Tropical Cyclones over Bay of Bengal with NCMRWF Regional Unified Model. *Pure and Applied Geophysics*, *174*(3), 1101–1119. https://doi.org/10.1007/s00024-016-1447-0

Saito, K., Fujita, T., Yamada, Y., Ishida, J., Kumagai, Y., Aranami, K., Ohmori, S., Nagasawa, R., Kumagai, S., Muroi, C., Kato, T., Eito, H., & Yamazaki, Y. (2006). The Operational JMA Nonhydrostatic Mesoscale Model. *Monthly Weather Review*, *134*(4), 1266–1298. https://doi.org/10.1175/MWR3120.1

Schade, L. R., & Emanuel, K. A. (1999). The Ocean's Effect on the Intensity of Tropical Cyclones: Results from a Simple Coupled Atmosphere–Ocean Model. *Journal of Atmospheric Sciences*, *56*(4), 642–651. https://doi.org/10.1175/1520-0469(1999)056<0642:TOSEOT>2.0.CO;2

Sengupta, D., Goddalehundi, B. R., & Anitha, D. S. (2008). Cyclone-induced mixing does not cool SST in the post-monsoon north Bay of Bengal. *Atmospheric Science Letters*, *9*(1), 1–6. https://doi.org/10.1002/asl.162

Shay, L. K., Goni, G. J., & Black, P. G. (2000). Effects of a Warm Oceanic Feature on Hurricane Opal. *Monthly Weather Review*, *128*(5), 1366–1383. https://doi.org/10.1175/1520-0493(2000)128<1366:EOAWOF>2.0.CO;2

Short, C. J., & Petch, J. (2017). How Well Can the Met Office Unified Model Forecast Tropical Cyclones in the Western North Pacific? *Weather and Forecasting*, *33*(1), 185–201. https://doi.org/10.1175/WAF-D-17-0069.1

Shu, S., Feng, X., & Wang, Y. (2018). Essential Role of Synoptic Environment on Rainfall Distribution of Landfalling Tropical Cyclones Over China. *Journal of Geophysical Research: Atmospheres*, *123*(20), 11,285-11,306. https://doi.org/10.1029/2018JD028842

Shultz, J. M., Russell, J., & Espinel, Z. (2005). Epidemiology of Tropical Cyclones: The Dynamics of Disaster, Disease, and Development. *Epidemiologic Reviews*, *27*(1), 21–35. https://doi.org/10.1093/epirev/mxi011

Singh, V., Konduru, R. T., Srivastava, A. K., Momin, I. M., Kumar, S., Singh, A. K., Bisht, D. S., Tiwari, S., & Sinha, A. K. (2021). Predicting the rapid intensification and dynamics of pre-monsoon extremely severe cyclonic storm 'Fani' (2019) over the Bay of Bengal in a 12-km global model. *Atmospheric Research*, *247*, 105222. https://doi.org/10.1016/j.atmosres.2020.105222

Srinivas, C. V., Mohan, G. M., Naidu, C. V., Baskaran, R., & Venkatraman, B. (2016). Impact of air-sea coupling on the simulation of tropical cyclones in the North Indian Ocean using a simple 3-D ocean model coupled to ARW. *Journal of Geophysical Research: Atmospheres*, *121*(16), 9400–9421. https://doi.org/10.1002/2015JD024431

Srinivas, C. V., Rao, D. V. B., Yesubabu, V., Baskaran, R., & Venkatraman, B. (2013). Tropical cyclone predictions over the Bay of Bengal using the high-resolution Advanced Research Weather Research and Forecasting (ARW) model. *Quarterly Journal of the Royal Meteorological Society*, *139*(676), 1810–1825. https://doi.org/10.1002/qj.2064

Subrahmanyam, B., Murty, V. S. N., Sharp, Ryan. J., & O'Brien, James. J. (2005). Air-sea Coupling During the Tropical Cyclones in the Indian Ocean: A Case Study Using Satellite Observations. *Pure and Applied Geophysics*, *162*(8), 1643–1672. https://doi.org/10.1007/s00024-005-2687-6

Sunder, S., Ramsankaran, R., & Ramakrishnan, B. (2020). Machine learning techniques for regional scale estimation of high-resolution cloud-free daily sea surface temperatures from MODIS data. *ISPRS Journal of Photogrammetry and Remote Sensing*, *166*, 228–240. https://doi.org/10.1016/j.isprsjprs.2020.06.008

Thakur, M. K., Kumar, T. V. L., Dwivedi, S., & Narayanan, M. S. (2018). On the rainfall asymmetry and distribution in tropical cyclones over Bay of Bengal using TMPA and GPM rainfall products. *Natural Hazards: Journal of the International Society for the Prevention and Mitigation of Natural Hazards*, *94*(2), 819–832.

Valdivieso, M., X. Feng and N. Klingaman (2020): Performance of Convective-Scale NWP for Oceanic Hazards and Air-Sea Interactions over the Bay of Bengal. WCSSP CASPER Deliverable Report 1.3, 22 pp, October 2020.

https://doi.org/10.5194/wcd-2021-46
Preprint. Discussion started: 26 July 2021

Valdivieso, M., N. Klingaman and C. Holloway (2021): Added Value of Atmospheric and Oceanic Resolutions for Predictions of Air-Sea Interactions in the Bay of Bengal. WCSSP CASPER Deliverable Report 2.2, 19 pp, March 2021.

Valcke, S., Craig, T., & Coquart, L. (2015). OASIS-MCT User Guide, CERFACS, Technical Report TR/CMGC/15/38.

Vecchi, G. A., & Soden, B. J. (2007). Effect of remote sea surface temperature change on tropical cyclone potential intensity. *Nature*, *450*(7172), 1066–1070. https://doi.org/10.1038/nature06423

Vellinga, M., Copsey, D., Graham, T., Milton, S., & Johns, T. (2020). Evaluating Benefits of Two-Way Ocean–Atmosphere Coupling for Global NWP Forecasts. *Weather and Forecasting, 35(5),* 2127–2144. https://doi.org/10.1175/WAF-D-20-0035.1

Vincent, E. M., Lengaigne, M., Madec, G., Vialard, J., Samson, G., Jourdain, N. C., Menkes, C. E., & Jullien, S. (2012). Processes setting the characteristics of sea surface cooling induced by tropical cyclones. *Journal of Geophysical Research: Oceans*, *117*(C2). https://doi.org/10.1029/2011JC007396

Walters, D., Baran, A. J., Boutle, I., Brooks, M., Earnshaw, P., Edwards, J., Furtado, K., Hill, P., Lock, A., Manners, J., Morcrette, C., Mulcahy, J., Sanchez, C., Smith, C., Stratton, R., Tennant, W., Tomassini, L., Van Weverberg, K., Vosper, S., … Zerroukat, M. (2019). The Met Office Unified Model Global Atmosphere 7.0/7.1 and JULES Global Land 7.0 configurations. *Geoscientific Model Development*, *12*(5), 1909–1963. https://doi.org/10.5194/gmd-12-1909-2019

Wang, Y., & Wu, C.-C. (2004). Current understanding of tropical cyclone structure and intensity changes – a review. *Meteorology and Atmospheric Physics*, *87*(4), 257–278. https://doi.org/10.1007/s00703-003-0055-6

Wu, L., Wang, B., & Braun, S. A. (2005). Impacts of Air–Sea Interaction on Tropical Cyclone Track and Intensity. *Monthly Weather Review*, *133*(11), 3299–3314. https://doi.org/10.1175/MWR3030.1

Xu, R., Tian, F., Yang, L., Hu, H., Lu, H., & Hou, A. (2017). Ground validation of GPM IMERG and TRMM 3B42V7 rainfall products over southern Tibetan Plateau based on a high-density rain gauge network. *Journal of Geophysical Research: Atmospheres*, *122*(2), 910–924. https://doi.org/10.1002/2016JD025418

Xu, W., Jiang, H., & Kang, X. (2014). Rainfall asymmetries of tropical cyclones prior to, during, and after making landfall in South China and Southeast United States. *Atmospheric Research*, *139*, 18–26. https://doi.org/10.1016/j.atmosres.2013.12.015

Yamaguchi, M., Ishida, J., Sato, H., & Nakagawa, M. (2017). WGNE Intercomparison of Tropical Cyclone Forecasts by Operational NWP Models: A Quarter Century and Beyond. *Bulletin of the American Meteorological Society*, *98*(11), 2337–2349. https://doi.org/10.1175/BAMS-D-16-0133.1

Yesubabu, V., Kattamanchi, V. K., Vissa, N. K., Dasari, H. P., & Sarangam, V. B. R. (2020). Impact of ocean mixed-layer depth initialization on the simulation of tropical cyclones over the Bay of Bengal using the WRF-ARW model. *Meteorological Applications*, *27*(1), e1862. https://doi.org/10.1002/met.1862

Yu, Z., Wang, Y., Xu, H., Davidson, N., Chen, Y., Chen, Y., & Yu, H. (2017). On the Relationship between Intensity and Rainfall Distribution in Tropical Cyclones Making Landfall over China. *Journal of Applied Meteorology and Climatology*, *56*(10), 2883–2901. https://doi.org/10.1175/JAMC-D-16-0334.1